Proton-Activated Chloride Channel 1 (PACC1) is essential for innate host defense against bacterial sepsis

Lucien P Garo[1,=], Kevin Brueck[1,2,=], Sarah Walachowski[1,2], Archana Jayaraman[1], Marcel Strueve[2], Shuang Xu[1], Hulbert Yang[1], Matthew Helmkamp[1], Seung Hoan Choi[3], Christoph Reinhardt[2,4,5], Markus Bosmann[1,2*]

[1]Pulmonary Center, Department of Medicine, Boston University Chobanian & Avedisian School of Medicine, Boston, MA, 02119, USA
[2]Center for Thrombosis and Hemostasis, University Medical Center of the Johannes Gutenberg-University Mainz, Mainz, 55131, Germany
[3]Department of Biostatistics, Boston University School of Public Health, Boston, MA, 02119, USA
[4]German Center for Cardiovascular Research (DZHK), Partner Site Rhine-Main, Mainz, 55131, Germany.
[5]Research Center for Immunotherapy (FZI), University Medical Center of the Johannes Gutenberg-University Mainz, Germany.

[=]L.G. and K.B. contributed equally

***Corresponding author:**
Markus Bosmann, Associate Professor of Medicine, Pathology & Laboratory Medicine, Pulmonary Center, Department of Medicine, Boston University Chobanian & Avedisian School of Medicine, Boston, Massachusetts, 02118, USA, Phone: +1-617-358-1225, FAX: +1-617-638-5227. E-mail: mbosmann@bu.edu

Author Contributions: LG, KB, MS, and SW conducted experiments, acquired and analyzed data. AJ analyzed data. SX, HY, and MH assisted with experiments. LG, KB, MS, and MB designed experiments. SHC advised regarding genetic association data. CR contributed tools and methods. All authors interpreted data. MB coordinated the studies. LG wrote the manuscript with KB, AJ, and MB, which was edited by CR.

Competing Interest Statement: The authors declare no competing financial interests.

Classification: Biological Sciences/Immunology and Inflammation

Keywords: Cytokines, immunology, innate immunity, infection

This PDF file includes:
Main Text
Figures 1 to 5

Abstract

Bacterial sepsis remains a devastating clinical problem. Here, we describe a protective role for the recently discovered acid-sensitive, proton-activated chloride channel, PACC1 (PAC/ASOR/TMEM206), during sepsis. Initially, we found PACC1 was enriched in healthy human and mouse mononuclear phagocytes, particularly macrophages, and differentially regulated by inflammatory stimuli, suggesting PACC1 involvement in innate immunity. To further investigate, we generated *de novo Pacc1* knockout ($^{-/-}$) mice, which presented without major immunologic abnormalities at baseline. Compared to wildtype (WT), *Pacc1*$^{-/-}$ myeloid cells showed normal phagocytic uptake of acid-insensitive *Escherichia coli BioParticles*, but impaired development of the acidifying phagolysosome using acid-sensitive *E. coli* BioParticles. Transcriptomic profiling of *Pacc1*$^{-/-}$ macrophages revealed dysregulated phagolysosomal and cytokine networks (e.g., interferons). Because phagolysosomal bacterial clearance is essential to resolve infection, we challenged *Pacc1*$^{-/-}$ mice with intraperitoneal gram-negative *E. coli* sepsis. *Pacc1*$^{-/-}$ mice displayed increased bacterial burden, immune cell infiltration, inflammation, and lethality. In contrast, phagocytosis-independent *E. coli* lipopolysaccharide (LPS)-induced endotoxemia yielded comparable WT and *Pacc1*$^{-/-}$ survival, as well as similar inflammatory responses. Finally, we engineered *Pacc1*-floxed ($^{fl/fl}$) mice crossed with a myeloid lineage Cre-deleter strain to interrogate myeloid cell-intrinsic PACC1 *in vivo*. Consistent with a predominate role for PACC1 during phagocytosis and bacterial clearance in these cells, *LysM-Cre/Pacc1*$^{fl/fl}$ mice exhibited impaired *E. coli* sepsis survival but indifferent endotoxemia phenotypes. In conclusion, PACC1 links sterilizing phagolysosomal activity with immune networks in sepsis pathobiology.

21 **Significance Statement**

22 Bacterial sepsis remains a major global health burden. Here, we report an essential role for the recently
23 discovered acid-sensitive chloride channel, PACC1 (PAC/ASOR/TMEM206), in protective host defense
24 during bacterial infection and sepsis. PACC1 is highly expressed in human and mouse phagocytic
25 myeloid cells, particularly macrophages, where it regulates phagocytic bacterial clearance and
26 inflammatory responses. Using *de novo* generated mice, we show that global or myeloid cell-targeted
27 deletion of PACC1 impairs development of phagolysosomal acidification, confers susceptibility to
28 bacterial infection and excessive inflammation, and undermines host defense. These findings warrant
29 further investigation of PACC1 in sepsis pathobiology.

30 **Main Text**

31

32 **Introduction**

33

34 Life-threatening bacterial infections are a devastating clinical problem, and the molecular
35 mechanisms of protective host defense require continued investigation. An estimated ~50 million annual
36 cases of sepsis worldwide have mortality rates of 20-50% (1). Strikingly, sepsis may account for up to
37 50% of US hospital deaths and is thought to be the most expensive condition affecting the US healthcare
38 system (2, 3). Pneumonia is a major risk factor for sepsis, causing approximately 50% of all cases (4)
39 and is itself a leading cause of death in children under five and in the elderly (5). Bacterial infections
40 cause the majority of sepsis deaths (6), despite a recent surge in viral sepsis due to COVID-19 (7). Gram-
41 negative *Escherichia coli* is a major pathogen of systemic bacteremia, especially in higher income
42 countries, and the gram-positive bacterium, *Streptococcus pneumoniae*, is the most common etiology of
43 bacterial pneumonia (8). Unfortunately, antibiotic resistance has been increasing amongst bacterial
44 pathogens, and infection-associated mortality in the US has not significantly improved since the
45 widespread use of antibiotics (6, 9). Treatment of bacterial infections is further complicated by limited
46 diagnostic capabilities—the exact infectious microbe remains unidentified in a plurality of bacterial sepsis
47 cases (6). Due to these ongoing public health threats, our laboratory (10-13) and many others (5, 14, 15)
48 have been investigating broadly applicable host defense mechanisms important for innate immune
49 responses to bacterial infections.

50 Tissue-resident macrophages mediate initial host defense against invading bacterial infections
51 and interface at mucosal/serosal sites (16). Phagocytosis by these surveilling macrophages and other
52 myeloid cells which are rapidly recruited to the site of infection, including neutrophils and monocytes, are
53 essential for preventing and limiting infection severity (17, 18). During phagocytosis, bacteria at the
54 plasma membrane are internalized in a receptor-mediated process into the membrane-bound
55 phagosome, which is followed by maturation and acidification of this compartment, culminating in fusion

56 with the acidic lysosome to form the phagolysosome. The strongly acidic pH of the phagolysosome and
57 a cocktail of proteolytic enzymes kill bacteria (17, 18). Thus, the study of host defense mechanisms
58 related to phagolysosomal development and function are of major relevance to bacterial infections.

59 Chloride is the most abundant free anion in humans and governs biological functions ranging from
60 intercellular signaling to intracellular vesicular acidification (19, 20). Decades of research has uncovered
61 many subtypes of cellular/intracellular membrane chloride channels and transporters (19). To cross
62 cellular membranes, chloride requires channels for passive diffusion, or specific proteins to actively
63 transport chloride in conjunction with other ions. Chloride channels/transporters have been linked to the
64 etiology of many diseases and implicated as therapeutic targets in cystic fibrosis, neurodegeneration,
65 epilepsy, osteopetrosis, hypertension, and infection (19, 20).

66 The molecular identity of a widely expressed acid-activated chloride channel, PACC1 (also known
67 as PAC, ASOR, TMEM2026) has recently been identified in two independent genome-wide siRNA
68 screens (21, 22), validating years of electrophysiological experimental data that had suggested the
69 existence of such a channel (21-25). PACC1 channels are homotrimers of TMEM206 subunits that each
70 contain two transmembrane domains (21, 22, 26-29). Mutagenesis and cryo-electron microscopy studies
71 have shown that all six transmembrane domains of the trimer participate in forming a chloride-selective
72 pore that is open upon acid-induced contraction of their extracellular/luminal domains (21, 22, 26-29).
73 This results in a steep pH dependence with PACC1 being closed at neutral pH and maximally activated
74 at pH 4.5, in addition to a steep voltage dependence (21-29).

75 Due to its unique acid sensitivity, studies initially focused on how PACC1 promotes acid-induced
76 cell death (21, 22, 25, 30, 31), particularly in the brain where PACC1 is highly expressed and where
77 extracellular pH can drop during ischemic stroke (30, 31). However, beyond acidosis, the role of PACC1
78 in health and disease remains largely unknown.

79 PACC1 is ubiquitously expressed and has been detected in all mammalian cells (21, 22). PACC1
80 is also highly evolutionarily conserved, with >90% conservation between mice and humans (21, 22),
81 suggesting essential biological functions. Beyond the established role of PACC1 in acidotoxicity, stroke,

82 and regulating responses to extracellular acidification (21, 22, 30, 32), its primary function may be the
83 regulation of intracellular vesicles whose acidic pH allows PACC1 activity (20, 33). Indeed, after its
84 identification, PACC1 has been characterized in these compartments (21, 22, 34-37) and recent studies
85 have identified a role for PACC1 in endosomal acidification and macropinosome resolution (34-37).

86 Here, we hypothesize PACC1 is essential in the phagolysosome, which contains a highly acidic
87 compartment optimal for PACC1 activation (28) with one of the highest concentrations of chloride (20).
88 We found PACC1 in macrophages is required for effective bacterial eradication, inflammatory responses,
89 and host resistance against sepsis.

Results

Human PACC1 is expressed abundantly in macrophages and other mononuclear phagocytes

PACC1 is ubiquitously expressed and has been detected in every mammalian cell type (21, 22). To explore where PACC1 may play a more predominant role, we first analyzed publicly available human single-cell RNA sequencing (scRNA-seq) data from the Human Protein Atlas (HPA) (38). The HPA scRNA-seq is based on 31 published datasets, and expression profiles were generated by converting read counts to normalized transcripts per million (nTPM). Amongst all cells, *PACC1* expression was highly enriched within immune cells (**Fig. 1A**). Moreover, within immune cells in peripheral blood, *PACC1* was preferentially expressed within phagocytic mononuclear myeloid cells, such as monocytes and dendritic cells, both in the HPA dataset (**Fig. 1B**), as well as by independent bulk RNA-seq datasets from the Immune Cell Atlas (**Fig. 1C**) (39). PACC1 was also highly elevated in glia, which include brain-resident microglial "professional" phagocytes, as well as astrocytes and oligodendrocytes with phagocytic capacity (**Fig. 1A**) (40). To determine whether PACC1 was likewise expressed in tissue-resident macrophages, the predominant mononuclear phagocytes that initially interface with bacteria during infection (12, 13, 15, 16, 41), we next examined HPA data from the 19 tissues with annotated tissue macrophage populations (**Fig. 1D**). *PACC1* was consistently enriched in immune cells compared to non-immune cells. Most strikingly, tissue macrophages were the highest *PACC1*-expressing cell type in almost every tissue. These included Kupffer cells and Hofbauer cells, which are specialized tissue macrophages in the liver and placenta, respectively; and Langerhans cells, which are specialized tissue macrophages/dendritic cells in the skin (16). In addition, HPA bulk RNA-seq data from 69 cell lines of various tissue origin revealed that myeloid lineage cell lines were enriched in the top 50% in terms of ranked *PACC1* expression (***SI Appendix,* Fig. S1A**). The highest *PACC1* expression was in THP-1 cells, and the third highest expression in U-937 cells, the most widely used cell lines for macrophage studies (42). In addition, we analyzed an expanded pool of cell lines that combined HPA bulk RNA-seq with data

116 from >1000 cell lines in the Cancer Cell Line Encyclopedia (CCLE) and a Genentech study (43). The top
117 2% of *PACC1*-expressing cells contained a plurality of myeloid lineage cells, including THP-1 cells (***SI***
118 ***Appendix,*** **Fig. S1B**).

119 To further assess whether PACC1 may be implicated in myeloid cell functions, we next analyzed
120 *PACC1* variant data from publicly available genome-wide association studies (GWAS). Although no
121 specific studies have functionally characterized any human *PACC1* genetic variants, we found multiple
122 GWAS have identified *PACC1* variant associations with myeloid cell-related phenotypes. According to
123 the Open Target GWAS aggregator (44), among all biological phenotypes associated with *PACC1*
124 variants, myeloid cell-related phenotypes were highly represented. "Monocyte counts" ranked as the most
125 supported phenotype (**Fig. 1E**). Closer examination revealed a modest but consistent pattern: most
126 *PACC1* variants were predicted to be loss-of-function (pLoF), and these pLoF variants were associated
127 with greater myeloid cell counts/frequencies, whereas the few predicted gain-of-function (pGoF) variants
128 were associated with the converse (***SI Appendix,*** **Table S1**). Furthermore, the recent large *All of Us*
129 (AoU) cohort revealed the association of septicemia with gene-level burden of low frequency *PACC1*
130 pLoF variants (**Fig. 1F**) (45). A separate large population cohort from the UK Biobank (46), which used a
131 broader assortment of clinical codes, showed an overall modest trend in association between *PACC1*
132 gene-level variant burden and several codes pertaining to predominantly bacterial infections (***SI***
133 ***Appendix,*** **Fig. S2**). In summary, these data demonstrate that *PACC1* expression in humans is highly
134 enriched in mononuclear phagocytes, particularly macrophages, and that *PACC1* variants may impact
135 myeloid cell biology and innate immunity.

136

137 *Pacc1 expression in mice is enriched in macrophages and other mononuclear phagocytes*

138

139 To further evaluate PACC1 in macrophages, we proceeded with mouse studies. We first sought
140 to determine whether *Pacc1* was also highly expressed in murine macrophages. Reanalysis of bulk RNA-
141 seq data from our previous sepsis study revealed *Pacc1* expression was ranked in the top 5% of all

142 genes in murine bone marrow-derived macrophages (BMDMs) at baseline (**Fig. 2A**) (11). Since
143 monoclonal antibodies for the PACC1 protein were not commercially available (47), we next employed
144 mRNA PrimeFlow (48) to specifically detect *Pacc1* mRNA across macrophage and splenocyte
145 populations by flow cytometry. As negative controls, we leveraged cells from our *de novo* generated
146 *Pacc1* knockout mice (***SI Appendix,* Fig. S3**), or WT cells without *Pacc1* target probe. Using this
147 PrimeFlow approach, robust *Pacc1* expression was first validated in murine BMDMs (**Fig. 2B**; gating
148 scheme in ***SI Appendix,* Fig. S4A**), as also recently confirmed at the protein level (35). Consistent with
149 human data (**Fig. 1B-C**), *Pacc1* expression in murine splenocytes was detectable in mononuclear
150 phagocytes, including macrophages, dendritic cells, and a small population of neutrophils, as well as B
151 cells, which also possess phagocytic capacity (18) (**Fig. 2C**; gating scheme in ***SI Appendix,* Fig. S4B**).
152 Overall, *Pacc1* was enriched in mononuclear phagocytes compared to other splenocytes (***SI Appendix,***
153 **Fig. S4C**). These findings were further corroborated by reverse transcription quantitative-PCR (RT-
154 qPCR) in fluorescence-activated cell (FAC)Sorted splenic myeloid cell populations, which showed higher
155 expression in macrophages, modest expression in monocytes, and detectable expression in
156 polymorphonuclear neutrophils (**Fig. 2D**). To ascertain PACC1 levels across a broader set of murine
157 tissue macrophages, we analyzed published transcriptomic data (49). Relevant to pneumonia and
158 peritoneal sepsis (16), *Pacc1* was highly expressed in peritoneal macrophages and alveolar
159 macrophages (**Fig. 2E**). Next, we analyzed single-nucleus sequencing data to examine the peritoneal
160 compartment. *Pacc1* was highly expressed within murine macrophages and other mononuclear
161 phagocytes, (including monocytes and dendritic cells), of naïve mice (**Fig. 2F-G**). Finally, we tested if
162 *Pacc1* in macrophages was differentially regulated in response to inflammatory stimuli associated with
163 infection, such as Toll-like receptor (TLR) ligands. In BMDMs, *Pacc1* expression was differentially
164 responsive to such stimuli (**Fig. 2H**). Of note, *Pacc1* was strongly downregulated by lipopolysaccharide
165 (LPS), a component of gram-negative bacterial cell walls (12). Direct stimulation of macrophages with
166 inactivated *E. coli* also inhibited *Pacc1* (**Fig. 2I**). Collectively, these data show that *Pacc1* expression is
167 abundant in human and mouse macrophages, and differentially regulated by inflammatory stimuli, further

168 supporting that PACC1 could be involved in innate immune responses to infection.

169

170 *De novo generation of Pacc1 knockout mice*

171

172 To further study the role of PACC1 *in vivo*, we generated mice with a global deletion of *Pacc1*
173 using a CRISPR/Cas-9 approach (***SI Appendix,* Fig. S3A**). Single-guide RNAs aligned to regions
174 flanking *Pacc1* exon 2 were injected into pronuclei/zygotes (C57BL/6J), resulting in a 120 base pair
175 deletion with a frame shift and a premature stop codon. This truncated exon was detectable by PCR (***SI***
176 ***Appendix,* Fig. S3B**). In addition, RT-qPCR for exons 2-8 verified absent *Pacc1* mRNA in macrophages
177 (***SI Appendix,* Fig. S3C**), suggesting nonsense-mediated mRNA decay (50). Acid-induced cytotoxicity
178 was lower in *Pacc1*$^{-/-}$ BMDMs (***SI Appendix,* Fig. S3D**), confirming loss of PACC1 protein function in line
179 with previous electrophysiology studies (21-25). In agreement with other independently generated mice
180 (21, 22), our *Pacc1*$^{-/-}$ strain was viable and fertile, displaying normal sex distributions, although the
181 frequency of homozygous offspring was slightly reduced from expected Mendelian ratios (25%) in
182 heterozygous breeding schemes (***SI Appendix,* Fig. S3E**). *Pacc1*$^{-/-}$ mice presented without gross
183 abnormalities. Males and females had normal body weights and clinical chemistry parameters including
184 blood proteins, metabolites, and electrolytes (***SI Appendix,* Fig. S3F-I**). Importantly, *Pacc1*$^{-/-}$ mice
185 housed under specific pathogen-free conditions showed no apparent immunologic abnormalities, with
186 normal numbers of peripheral myeloid and lymphoid cells in the blood and spleen (***SI Appendix,* Fig.**
187 **S3J-L**, gating scheme in ***SI Appendix,* Fig. S5**). Together, these data suggest that *Pacc1*$^{-/-}$ mice lack
188 developmental immunologic abnormalities, making them appropriate to study bacterial infections *in vivo*.

189

190 *Pacc1*$^{-/-}$ *mice have defective development of phagolysosomal acidification in vitro and in vivo*

191

192 Acid-triggered PACC1 may play an active role in the acidifying phagolysosome of myeloid cells
193 (28). To study if bacteria induce PACC1-containing phagosomes in macrophages, we re-analyzed

194 published proteomic data: Li *et al.* used an engineered ascorbate peroxidase (APEX)-based proximity
195 labeling technique combined with mass spectrometry in murine macrophages to identify phagosomal
196 host proteins following phagocytosis of APEX-tagged inactivated gram-negative *E. coli* and gram-positive
197 *Staphylococcus aureus* (51). Indeed, PACC1 protein was enriched in bacteria-containing phagosomes
198 in BMDMs (**Fig. 3A**). Next, we tested the development of phagolysosomal acidification in *Pacc1*$^{-/-}$ mice
199 using inactivated *E. coli* BioParticles conjugated with an acid-sensitive fluorophore. These phagocytosed
200 BioParticles become fluorescent at low pH as the phagosome fuses with the lysosome (52). We found
201 BioParticles incubated with *Pacc1*$^{-/-}$ BMDMs displayed decreased fluorescence compared to WT
202 counterparts (**Fig. 3B**). These data suggested a defect in the development of the acidifying
203 phagolysosome, as normal phagocytic engulfment of synthetic beads by macrophages has been reported
204 not to require PACC1 (35), in accordance with PACC1 inactivity at neutral plasma membrane pH (22, 26-
205 29). We also confirmed normal phagocytic uptake of *E. coli* cargo in *Pacc1*$^{-/-}$ macrophages by exposure
206 to acid-insensitive Alexa Fluor (AF)488-conjugated *E. coli* BioParticles. AF488-*E. coli* emit a stable signal
207 from pH 3-10 independent of phagolysosomal acidification (53). AF488 fluorescence in *Pacc1*$^{-/-}$
208 macrophages was indistinguishable from WT, and signals in both strains were abrogated by cytochalasin
209 D, an inhibitor of actin polymerization and phagocytic uptake (53, 54) (**Fig. 3C-D**). Accordingly, *Pacc1*$^{-/-}$
210 macrophages exhibited impaired intracellular killing of live pathogenic *E. coli*, while levels of extracellular
211 bacteria were comparable to WT cultures (**Fig. 3E**), indicating intact phagocytic uptake but defective
212 phagolysosomal killing. When acid-sensitive *E. coli* BioParticles were injected intraperitoneally (i.p.) in
213 mice, a similar reduction in fluorescence in *Pacc1*$^{-/-}$ vs. WT myeloid cells was noted (**Fig. 3F-G**).
214 Additionally, *Pacc1*$^{-/-}$ mice displayed heightened inflammatory responses to inactivated BioParticles,
215 characterized by increased recruitment of myeloid cells to the peritoneum, including monocytes and
216 monocyte-derived macrophages (**Fig. 3H**, gating scheme in ***SI Appendix,* Fig. S6**). IL-6, a major pro-
217 inflammatory cytokine (12), was also elevated in peritoneal lavage fluid of *Pacc1*$^{-/-}$ mice injected with
218 BioParticles (**Fig. 3I**). In contrast, no aberrant signs of pre-existing inflammation were present in the
219 peritoneum of naïve *Pacc1*$^{-/-}$ mice (***SI Appendix,* Fig. S7**), consistent with immunoprofiling in the

220 periphery (***SI Appendix,* Fig. S3J-L**). Both naïve WT and *Pacc1*$^{-/-}$ mice had low numbers of infiltrating
221 peritoneal monocytes and neutrophils, with modestly fewer monocytes in *Pacc1*$^{-/-}$ mice (***SI Appendix,***
222 **Fig. S7A-B**); and IL-6 was undetectable in both strains (***SI Appendix,* Fig. S7C**). As a whole, these data
223 suggest acidification of the phagolysosome is defective in *Pacc1*$^{-/-}$ myeloid cells, and that PACC1
224 deficiency may result in hyperinflammation following bacterial challenge.
225
226 *Pacc1*$^{-/-}$ *macrophages have dysregulated immunologic and phagolysosomal transcriptomic responses*
227
228 To screen for the transcriptome-wide effects of *Pacc1* loss on host defense and phagolysosomal
229 pathways, we sequenced RNA from BMDMs stimulated with *E. coli* BioParticles. Principal component
230 analysis revealed strong segregation based on *E. coli* stimulation, as well as segregation based on
231 genotype (**Fig. 4A**). *Pacc1*$^{-/-}$ control compared to WT control samples were distinguishable at baseline
232 and further segregated following phagocytic stimulation. *E. coli* triggered robust transcriptomic activity,
233 with >10,000 significant differentially expressed genes (DEGs) in each group of WT and *Pacc1*$^{-/-}$
234 macrophages (***SI Appendix,* Fig. S8A-C; Dataset S1**). In response to *E. coli*, *Pacc1*$^{-/-}$ vs. WT
235 macrophages displayed 2,162 upregulated and 1,795 downregulated DEGs (**Fig. 4B**). WT and *Pacc1*$^{-/-}$
236 macrophages also displayed a smaller proportion of DEGs at baseline (***SI Appendix,* Fig. S8D**);
237 however, the majority were uniquely dysregulated by *E. coli* (**Fig. 4C**).
238 To assess global changes, we performed a gene set enrichment analysis (GSEA) for hallmark
239 biological processes using both significant and non-significant DEGs. Immunologic gene sets were
240 differentially enriched in *Pacc1*$^{-/-}$ vs. WT macrophages both at baseline (***SI Appendix,* Fig. S9A; Dataset**
241 **S2**) and following *E. coli* phagocytosis (**Fig. 4D; *SI Appendix,* Dataset S2**), including TNF-α via NFκB
242 signaling (***SI Appendix,* Fig. S9B-C**) and interferon responses (***SI Appendix,* Fig. S9D-G**), as well as
243 JAK/STAT signaling (***SI Appendix,* Fig. S9A, H**). Further analysis via the "Interferome database", a
244 curated list of empirically determined interferon-responsive genes (55), revealed strong dysregulation of

245 type I and II interferon signaling in *Pacc1*$^{-/-}$ macrophages following bacterial challenge (***SI Appendix,* Fig.**
246 **S10**).

247 Ingenuity Pathway Analysis (IPA) identified dysregulated signaling in *Pacc1*$^{-/-}$ macrophages in
248 response to *E. coli* (***SI Appendix,* Dataset S3**). Notably, the "pathogen-induced cytokine storm signaling
249 pathway" was one of the most highly upregulated pathways in *Pacc1*$^{-/-}$ vs. WT macrophages (**Fig. 4E**).
250 Uncontrolled cytokine release is a leading contributor to death in sepsis patients (15). DEGs enriched in
251 this pathway resolved that this activation response was not uniform: expression of some inflammatory
252 mediators were elevated in *Pacc1*$^{-/-}$ vs. WT macrophages following *E. coli* exposure (e.g., *Il1rap, Ccl6*,
253 *Pf4, Ripk1, Jak1, Stat3, Tlr9, Tlr3, Cgas, Nod1,* and *Sting1*), while others were downregulated (e.g., *Il6*,
254 *Il1b*, *Cxcl1*, and *Cxcl2*).

255 Next, to study dysregulated biological processes in *Pacc1*$^{-/-}$ macrophages at a more granular
256 level, including phagolysosomal functions, we analyzed the enrichment of gene ontology biological
257 processes (GOBPs) for significant DEGs (***SI Appendix,* Dataset S4**). Amongst the top upregulated
258 GOBPs, a majority were associated with either innate immunity or intracellular vacuoles/vesicles (**Fig.**
259 **4F**). More than 100 DEGs were enriched in "regulation of innate immune response" processes in *Pacc1*$^{-}$
260 $^{/-}$ vs. WT macrophages, the majority of which were associated with positive regulation, both following *E.*
261 *coli* incubation and at baseline (***SI Appendix,* Fig. S11**). In contrast, the top downregulated pathways in
262 *Pacc1*$^{-/-}$ vs. WT macrophages during phagocytosis were related predominantly to RNA processing (***SI***
263 ***Appendix,* Fig. S12**).

264 To determine if *Pacc1* loss affected downstream phagolysosomal regulation, we manually curated
265 a list of annotated processes. Consistent with an important role for PACC1 during bacterial challenge,
266 multiple GOBPs associated with lysosomal activity were differentially regulated in *Pacc1*$^{-/-}$ vs. WT
267 macrophages (e.g., lysosomal organization/transport, lysosomal lumen acidification; adj. $P<0.1$), while
268 differences in GOBPs associated with early phagocytic processes (e.g., engulfment) were not significant
269 (**Fig. 4G**). Interestingly, a majority of these enriched DEGs were upregulated (**Fig. 4H**), which may
270 indicate a potential transcriptomic compensatory response for the defective phagolysosomal acidification

271 in *Pacc1*$^{-/-}$ macrophages (**Fig. 3B-G**). A subset of phagolysosomal processes were also dysregulated at
272 baseline in *Pacc1*$^{-/-}$ compared to WT macrophages (***SI Appendix,* Fig. S13**), suggesting unexpected
273 PACC1 activity in resting cells. In summary, these findings indicate that loss of *Pacc1* in macrophages
274 results in transcriptomic dysregulation in immunological and phagolysosomal pathways, particularly in
275 response to phagocytotic bacterial stimulus.
276
277 *Pacc1 knockout mice and myeloid cell-targeted conditional Pacc1 knockout mice are susceptible to E.*
278 *coli sepsis*.
279
280 Because defective phagolysosomal acidification inhibits pathogen clearance (17, 18), we next
281 studied if *Pacc1*$^{-/-}$ mice were susceptible to bacterial infections. In an established *E. coli* sepsis model
282 (11) (**Fig. 5A**), *Pacc1*$^{-/-}$ mice succumbed to severe mortality (**Fig. 5B**). In contrast to 100% of WT
283 counterparts, only 50% of *Pacc1*$^{-/-}$ mice survived. This increased lethality was associated with
284 significantly higher bacterial burden in peritoneal lavage (**Fig. 5C**) and systemic bacteremia (**Fig. 5D**,
285 gating scheme in ***SI Appendix,* Fig. S14A**). Moreover, a greater inflammatory response in *Pacc1*$^{-/-}$ mice
286 was indicated by increased myeloid cell infiltration (**Fig. 5E,** gating scheme in ***SI Appendix,* Fig. S14B**)
287 and IL-6 release in peritoneal lavage fluid (**Fig. 5F**). However, this enhanced compensatory response
288 was apparently unable to clear infection. In conclusion, these data suggest *Pacc1*$^{-/-}$ mice are susceptible
289 to bacterial infection and dysregulated inflammation, which may be explained by defective myeloid cell
290 responses.
291 Next, to test whether this susceptibility of *Pacc1*$^{-/-}$ mice to a gram-negative bacterial infection in
292 the peritoneum (**Fig. 5A-F**) was broadly applicable, we examined susceptibility in a gram-positive
293 pneumonia setting (56). Mice were intranasally (i.n.) inoculated with S. *pneumoniae* (***SI Appendix,* Fig.**
294 **S15A**). As with *E. coli* sepsis, *Pacc1*$^{-/-}$ mice experienced significantly higher mortality (***SI Appendix,* Fig.**
295 **S15B**), greater peak weight loss (***SI Appendix,* Fig. S15C**), and more lung injury as indicated by

296 bronchoalveolar protein leakage (***SI Appendix,* Fig. S15D**). Accordingly, *Pacc1*$^{-/-}$ mice tended to have
297 an elevated bacterial burden (***SI Appendix,* Fig. S15E**). Like *E. coli* sepsis, pneumococcal pneumonia
298 induced more pronounced local myeloid cell infiltration in bronchoalveolar lavages from *Pacc1*$^{-/-}$ mice (***SI***
299 ***Appendix,* Fig. S15F**, gating scheme in **Fig. S16**). This was accompanied by a general elevation of
300 inflammatory mediators (***SI Appendix,* Fig. S15G-H**), including IL-6 as well as IFN-γ, a cytokine important
301 for macrophage activation and bacterial clearance (5, 15, 57). In contrast, we found no signs of pulmonal
302 inflammation at baseline in naïve *Pacc1*$^{-/-}$ mice (***SI Appendix,* Fig. S17**), which was consistent with
303 immunoprofiling in other sites (***SI Appendix,* Fig. S3J-L, S7**). We noted an elevation in homeostatic
304 numbers of alveolar macrophages in *Pacc1*$^{-/-}$ mice (***SI Appendix,* Fig. S17A-B**), which could represent
305 a potential compensatory response for their phagocytic defects. Like WT, naive *Pacc1*$^{-/-}$ mouse lungs
306 displayed low numbers of infiltrating monocytes and neutrophils (***SI Appendix,* Fig. S17A-B**), and
307 undetectable levels of IL-6 (***SI Appendix,* Fig. S17C**). Overall, these data suggest *Pacc1*$^{-/-}$ mice are
308 susceptible to bacterial infection and trigger hyperinflammation associated with defective myeloid cells in
309 this context.

310 To further explore if severe mortality and inflammation in septic *Pacc1*$^{-/-}$ mice was specifically
311 dependent on phagocytosis, we induced sterile endotoxemia by i.p. injection of *E. coli*-derived LPS (**Fig.**
312 **5G**). In contrast to live *E. coli*, LPS activates TLR4 without phagocytic uptake (12). High-dose LPS
313 resulted in 100% mortality (**Fig. 5H**), while medium-dose LPS led to approximately 50% mortality (**Fig.**
314 **5I**). Survival curves for *Pacc1*$^{-/-}$ and WT mice were identical at both titrations, indicating PACC1 is not
315 essential for phagocytosis-independent inflammatory responses. Accordingly, IL-6 concentrations were
316 comparable between strains (**Fig. 5J**). Transcriptional analysis of *Pacc1*$^{-/-}$ BMDMs following LPS
317 stimulation *in vitro* also confirmed responses were indistinguishable from WT (***SI Appendix,* Fig. S18**).

318 Although *PACC1* is enriched in macrophages (**Fig. 1-2**), its expression remains ubiquitous (**Fig.**
319 **1**), challenging the assignment of a causal role for PACC1 in macrophages during bacterial sepsis. To
320 evaluate PACC1 loss in specific cell types during *in vivo* infection, we initiated the *de novo* generation of

321 *Pacc1-floxed* $^{(fl/fl)}$ mice via CRISPR/Cas9 (**Fig. 5K**). The expected elongated bands in *Pacc1*$^{fl/fl}$ mice that
322 received loxP insertions were detectable by PCR (***SI Appendix,* Fig. S17A**). As expected, *Pacc1*$^{fl/fl}$ mice
323 showed unchanged *Pacc1* expression in peritoneal cells before Cre-mediated recombination (***SI***
324 ***Appendix,* Fig. S17B**). *Pacc1*$^{fl/fl}$ mice crossed with *LysM-Cre* mice (58) for myeloid cell-targeted deletion
325 showed >90% deletion in peritoneal tissue macrophages (**Fig. 5L**, gating scheme in ***SI Appendix,* Fig.**
326 **S17C**). Crucially, these conditional knockout mice recapitulated the high sepsis mortality in global *Pacc1*$^{-}$
327 $^{/-}$ (**Fig. 5M**), which was similarly associated with greater peritoneal bacterial burden (**Fig. 5N**).
328 Furthermore, in low-dose endotoxemia to detect potentially subtle sensitivity differences, myeloid cell-
329 targeted *Pacc1* deletion did not impact survival (**Fig. 5O**) or peripheral blood and immune cell parameters
330 (**Fig. 5P-Q**), further implicating PACC1 in phagocytosis-mediated immunity. In conclusion, PACC1
331 promotes protective host responses, as PACC1 deficiency within myeloid cells undermines anti-bacterial
332 defense mechanisms and weakens resistance to sepsis and pneumonia.

333 **Discussion**

334

335 Bacterial sepsis remains a major health burden (1). Our study has identified the recently
336 discovered acid-sensitive chloride channel, PACC1 (also known as PAC, ASOR, TMEM206) (21, 22), as
337 a regulator of host defense against bacterial infections and sepsis. PACC1 was highly expressed within
338 human and mouse phagocytic myeloid cells, particularly macrophages, where it controlled sepsis
339 outcomes. Using *de novo*-generated mice, *Pacc1* knockout globally or in myeloid cells impaired
340 development of phagolysosomal acidification and conferred susceptibility to bacterial infection and
341 excessive inflammation.

342 While PACC1 is uniquely activated under acidic conditions, its ubiquitous expression has
343 obscured its physiological roles (21, 22). The data we have presented showing elevated *PACC1* in human
344 and murine macrophages, along with GWAS data linking *PACC1* variants with myeloid cell phenotypes,
345 suggest PACC1 is relevant for macrophage responses. Our re-analysis of proteomic data from Li *et al.*
346 (51) confirmed PACC1 localized to bacteria-containing phagosomes in primary macrophages, although
347 the lack of reliable, commercial monoclonal PACC1 antibodies constrained further experimental protein
348 detection (47). These data are consistent with other systems using in-house generated PACC1
349 antibodies or reporters that show PACC1 colocalizes strongly with early endosomal and partially with late
350 endosomal/lysosomal markers in BMDMs and cell lines (32, 34, 35). Recently, PACC1 expression has
351 been reported in osteoclasts, a specialized multi-nucleated macrophage (32). Our findings explicitly
352 identified elevated *Pacc1* in murine tissue macrophages and other primary immune cells *in vivo.* Our data
353 also showed *Pacc1* expression in macrophages was dynamically regulated by diverse inflammatory
354 stimuli. This suggests context-specific roles for PACC1 in infection that adapt to local milieus. For
355 example, PACC1 downregulation at the plasma membrane may promote cell survival against
356 extracellular acidic environments during inflammation/infection (21, 22, 30, 31).

357 Our view that PACC1 is essential for microbial phagocytosis and related endo/exo/pinocytic
358 processes is shared by others (32, 34-37, 59). However, the contextual outcomes of *Pacc1* loss may

359 depend on specific cell types, cargos, and other factors. For example, while PACC1 may limit endosomal
360 acidification during transferrin recycling in cell lines and receptor trafficking in neurons (34, 36), we found
361 PACC1 facilitates acidification in macrophage phagolysosomes. This may occur via the influx of chloride
362 which acts as a negative electrical shunt to permit proton pumping that drives acidification (20, 33). While
363 PACC1 is typically outwardly rectifying, it is a passive channel, and thus chloride transit depends on local
364 electrochemical gradients (21-29). Of note, the chloride anion shunt hypothesis remains debated (20).
365 Studies have suggested chloride is dispensable for lysosomal acidification (60, 61) and serves functions
366 beyond shunting (20). There remains ambiguity around even the most well-studied chloride channel,
367 cystic fibrosis transmembrane conductance regulator (CFTR). Multiple groups have reported CFTR is
368 required for intracellular acidification, while others have shown no effect on acidification and macrophage
369 bacterial clearance (20, 33, 62, 63). Posited explanations include differences in CFTR knockout,
370 inhibition, or mutations; differences in human and mouse primary cells and cell lines; and differences in
371 protocols and models (20, 33, 62, 63). Most recently, Badr *et al*. suggested bacterial cargo is critical, as
372 CF patient macrophages display defective lysosomal acidification following phagocytosis of *Burkholderia*
373 *cenocepacia*, but not *E. coli* (64). Further work is needed to clarify the nuanced context-dependent roles
374 of chloride in vesicular acidification, as well as the specific biophysical mechanisms undermining the
375 acidifying phagolysosome in *Pacc1*$^{-/-}$ macrophages.

376 In the present study, transcriptomic profiling of *Pacc1*$^{-/-}$ macrophages exposed to inactivated *E.*
377 *coli* revealed dysregulated immunologic functions. Consistent with our hypothesis that PACC1 is critical
378 for phagolysosomal activity, lysosomal processes were highly dysregulated in *Pacc1*$^{-/-}$ macrophages;
379 while processes associated with early phagocytosis (e.g., engulfment) were largely unaffected. The
380 observed upregulation of lysosomal processes in *Pacc1*$^{-/-}$ macrophages was unexpected. In contrast, we
381 observed defective phagolysosomal activity using acid-sensitive fluorescent *E. coli* BioParticles, and
382 corresponding host defense impairments against live bacteria. It is possible transcriptomic upregulation
383 of lysosomal processes represents a compensatory response. *Pacc1*$^{-/-}$ macrophages also displayed
384 enhanced signaling from endolysosomal TLRs that respond to phagocytosed bacteria (17, 18). Impaired

385 acidification may have caused inefficient cargo degradation which extended ligand–receptor contact. The
386 "extended contact" hypothesis (65) acknowledges that while some acidification is required for
387 endolysosomal TLR activation (66), partial defects can enhance signaling (65). Innate immune activation
388 in *Pacc1*$^{-/-}$ macrophages was heterogenous, with both positive and negative regulation of various
389 inflammatory markers, indicating PACC1 may differentially regulate inflammatory pathways via distinct
390 mechanisms that deserve future study. Unexpectedly, we found *Pacc1*$^{-/-}$ macrophages displayed certain
391 transcriptomic perturbations at baseline, despite the absence of overt abnormalities in naive mice (21,
392 22, 32). This may reflect homeostatic phago/efferocytosis (16-18), or possibly non-canonical roles for
393 PACC1 (47, 67-74), as has been described for other chloride channels (75, 76).

394 Interestingly, we observed some differential inflammatory responses between *Pacc1*$^{-/-}$ vs. WT
395 BMDMs challenged *in vitro* with inactivated *E. coli* compared to mice *in vivo* with live or inactivated *E. coli*
396 (e.g. IL-6 production). This may be due to differences from tissue macrophage populations, differences
397 from live bacterial burdens, as well as differences from the inflammatory milieu *in vivo* including infiltrating
398 myeloid cells. *Pacc1* deficiency did not affect LPS-induced IL-6 production and low baseline IL-6 levels
399 in mice. The present findings support that elevated IL-6 in *Pacc1*$^{-/-}$ mice challenged with bacteria reflects
400 the particular *in vivo* inflammatory context rather than discrepant baseline macrophage-intrinsic
401 responses.

402 The predominant impact of PACC1 during sepsis appeared dependent on phagocytosis. LPS,
403 which activates TLR4 independent of phagocytosis (12), resulted in *Pacc1*$^{-/-}$ endotoxemia survival
404 comparable to WT. Conversely, in line with impaired phagolysosomal acidification, *Pacc1*$^{-/-}$ mice exposed
405 to live bacteria showed increased bacterial burdens and sepsis susceptibility. The augmented neutrophil
406 recruitment in septic *Pacc1*$^{-/-}$ mice may have served as a compensatory response when tissue-resident
407 macrophages failed to control bacterial pathogens during early infection (5, 15). Although heightened
408 inflammation likely reflects increased bacterial burden, *Pacc1*$^{-/-}$ myeloid cells also displayed intrinsic
409 hyperresponsiveness to bacterial challenge, as evidenced by exaggerated cytokine responses to
410 inactivated *E. coli*. The translational relevance of these findings was supported by congruence with

411 human genetic data. Predicted loss-of-function *PACC1* variants were associated with increased myeloid
412 cell counts and risk for septicemia and various bacterial infections, reflecting the phenotype observed in
413 *Pacc1*$^{-/-}$ mice during live infection. In our myeloid cell-targeted *LysM-Cre*/*Pacc1*$^{fl/fl}$ mice, sepsis
414 susceptibility was recapitulated while endotoxemia outcomes remained unaltered. These findings further
415 validated that PACC1 mediates phagolysosomal bacterial clearance via action within macrophages,
416 monocytes, and neutrophils. Although PACC1 expression is greater in mononuclear phagocytes,
417 including tissue macrophages that first encounter pathogens, recruited neutrophils become the
418 predominant myeloid cell type (5, 16). *Pacc1*$^{-/-}$ neutrophils also exhibited defective development of the
419 acidifying phagolysosome in response to *E. coli* BioParticles *in vivo*. Future studies should elaborate on
420 the direct role of PACC1 in other PACC1-expressing immune cells. Of note, human pLoF *PACC1* variants
421 were associated with increased myeloid cell counts and risk for septicemia and bacterial infections,
422 supporting the translationally relevance of our findings. Unfortunately, only limited studies have been
423 conducted in PACC1-overexpressing cell lines *in vitro* (21, 59, 77, 78), and there are no known specific
424 PACC1 agonists to test if augmenting PACC1 is therapeutic during sepsis *in vivo* (77).

425 In parallel to our work, Cheng *et al.* also recently studied PACC1 in macrophages during infection
426 (59). Both studies suggest PACC1 is crucial for phagolysosomal acidification, bacterial clearance,
427 inflammation, and sepsis outcomes (59). Both indicate PACC1 is abundant in macrophages and
428 downregulated by LPS, with *Pacc1*$^{-/-}$ macrophages showing increased interferon and other inflammatory
429 signaling following bacterial challenge, though no change following LPS (59). Although Cheng *et al.*
430 suggest enhanced acidification during phagocytosis releases more bacterial ligands to enhance
431 immunologic signaling (59), partial defects in acidification may also enhance signaling by extending
432 ligand contact (65).

433 While our study characterized defective phagolysosomal acidification, decreased survival, and
434 hyperinflammation in *Pacc1*$^{-/-}$ mice following bacterial infection, Cheng *et al.* reported the converse (59).
435 This divergence may arise from differences in mouse strains, pathogens, and methods. For example, we

436 employed independently generated *Pacc1*-deficient strains with strict genetic/microbiome controls (59,
437 79, 80). We speculate evolutionary conserved PACC1 (21, 22) may be a target of microbial evasion
438 strategies and pathogenicity factors that could modulate its activity, potentially explaining *E. coli* strain-
439 dependent differences between studies (59). Our findings in both gram-negative peritoneal infection and
440 gram-positive lung infection support relevance across bacterial contexts, as does congruence with human
441 data linking pLoF *PACC1* variants with increased myeloid cell counts and sepsis risk. Discrepant results
442 between studies may also stem from differences in cell types, time points, and cargo (64) (e.g., Cheng
443 *et al*. used zymosan-conjugated particles (59), while we employed *E. coli*).

444 Most PACC1 functional studies have focused on direct electrophysiological conductance of
445 chloride (21, 22, 26-28, 30, 34, 35, 81), though some suggest complex context-dependent and potentially
446 non-canonical chloride-independent PACC1 functions (74). For example, recent work suggests PACC1
447 decreases acid-induced death in colorectal cancer cells (68, 69), diverging from findings by us and others
448 (21, 22, 25, 30, 31). PACC1 may have direct protein binding/signaling partners (47, 67). PACC1 has
449 been implicated in the opposing cancer processes of proliferation and migration (68-72, 82), and at non-
450 acidic pH may mediate ophthalmic pathology (73). Interestingly, both we and Cheng *et al.* (59) identified
451 in *Pacc1*$^{-/-}$ macrophages dysregulated RNA processing for which the role of chloride remains undefined.
452 In total, findings from this and prior studies underscore the context-dependent and multifaceted functions
453 of PACC1.

454 In conclusion, our results demonstrate a novel role for PACC1 in protective host defense and
455 warrant further studies on PACC1 during sepsis and other bacterial infections.

456 **Materials and Methods**

457

458 All the materials used in this study, including sources for reagents, and detailed methodologies
459 for the generation of mouse strains, BMDM assays, analysis of splenocytes and blood, *E. coli* BioParticle
460 assays, *E. coli* sepsis, pneumococcal pneumonia, endotoxemia, flow cytometry, protein detection, RT-
461 qPCR, bulk and single-cell/nucleus transcriptomics, proteomics, and GWAS, and statistical analyses, are
462 in the ***SI Appendix***, Materials and Methods.

463

464 **Acknowledgments**

465

466 This work was supported by the Federal Ministry of Education and Research (01EO1503 to MB),
467 the Deutsche Forschungsgemeinschaft (BO3482/3-3, BO3482/4-1 to MB), the National Institutes of
468 Health (1R01HL141513, 1R01HL139641, 1R01HL166588 to MB; F31HL176388-01A1 to LG;
469 5T32HL007035-50 supported the training of LG). CR is a member at the German Center for
470 Cardiovascular Research (DZHK), the DFG Research Unit 5644 INFINITE (RE 3450/15-1), the Center
471 for Translational Vascular Biology, the Research Center for Immunotherapy (FZI), and Potentialbereich
472 EXPOHEALTH, and received a Fellowship from the Gutenberg Research College. We cordially thank Dr.
473 Thomas J. Jentsch for collaborative efforts and Dr. Kara Vasilew for assistance. We also thank the Flow
474 Cytometry Core of Boston University School of Medicine (S10 OD038346) and Shari Brezinsky for
475 assistance. The authors are responsible for the contents of this publication.

476 **Data, Materials, and Software Availability**

477

478 Single-nucleus multiome sequencing data from our previous study is available in the NCBI Gene
479 Expression Omnibus (GEO) repository (accession code: GSE269703; reviewer access token:
480 wbcxyyaahfandwz). Only data pertaining to unstimulated cells were used here. Bulk RNA-seq data from
481 this study is available in GEO (accession code: GSE292930; reviewer access token: yjinyuiihnyjpep).
482 Phenotypes associated with human *PACC1* variants were from Open Targets
483 (https://platform.opentargets.org/) (44). Genetic association data for *PACC1* variants in the All of Us
484 Biobank were from Jurgens *et al.* browser
485 (https://hugeamp.org:8000/research.html?pageid=600_traits_app_home) (45) and the UK Biobank from
486 Genebass (https://app.genebass.org/) (46). *PACC1* expression from human single-cell and bulk RNA-
487 seq data were from the HPA (https://www.proteinatlas.org/) (38) and Immunological Genome Project ICA
488 (http://immunecellatlas.net/ICA_Skyline.php) (39). Data from published studies (11, 49, 51) were from
489 respective source/supplementary data. This paper reports no original code. Additional information is
490 available from the corresponding author upon request.

491

Figures and Captions

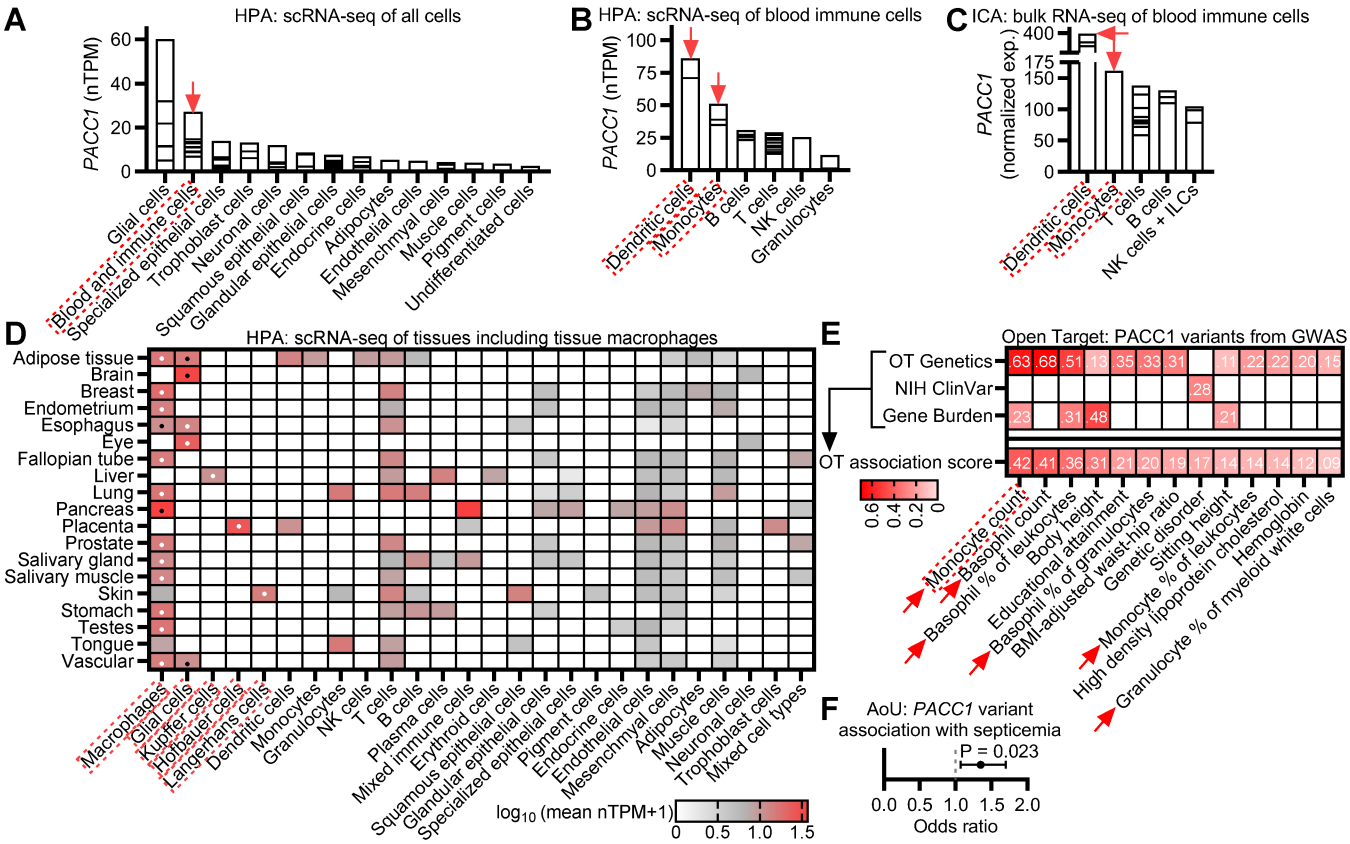
A
HPA: scRNA-seq of all cells
PACC1 (nTPM)
60
40
20
0
Glial cells
Blood and immune cells
Specialized epithelial cells
Trophoblast cells
Neuronal cells
Squamous epithelial cells
Glandular epithelial cells
Endocrine cells
Adipocytes
Endothelial cells
Mesenchmyal cells
Muscle cells
Pigment cells
Undifferentiated cells
B
HPA: scRNA-seq of blood immune cells
PACC1 (nTPM)
100
75
50
25
0
Dendritic cells
Monocytes
B cells
T cells
NK cells
Granulocytes
C
ICA: bulk RNA-seq of blood immune cells
PACC1 (normalized exp.)
400
175
150
100
50
0
Dendritic cells
Monocytes
T cells
B cells
NK cells + ILCs
D
HPA: scRNA-seq of tissues including tissue macrophages
Adipose tissue
Brain
Breast
Endometrium
Esophagus
Eye
Fallopian tube
Liver
Lung
Pancreas
Placenta
Prostate
Salivary gland
Salivary muscle
Skin
Stomach
Testes
Tongue
Vascular
Macrophages
Glial cells
Kupffer cells
Hofbauer cells
Langerhans cells
Dendritic cells
Monocytes
Granulocytes
NK cells
T cells
B cells
Plasma cells
Mixed immune cells
Erythroid cells
Squamous epithelial cells
Glandular epithelial cells
Specialized epithelial cells
Pigment cells
Endocrine cells
Endothelial cells
Mesenchmyal cells
Adipocytes
Muscle cells
Neuronal cells
Trophoblast cells
Mixed cell types
log10 (mean nTPM+1)
0
0.5
1.0
1.5
E
Open Target: PACC1 variants from GWAS
OT Genetics
NIH ClinVar
Gene Burden
OT association score
.63 .68 .51 .13 .35 .33 .31 .11 .22 .22 .20 .15
.28
.23 .31 .48 .21
.42 .41 .36 .31 .21 .20 .19 .17 .14 .14 .14 .12 .09
0.6
0.4
0.2
0
Monocyte count
Basophil count
Basophil % of leukocytes
Body height
Educational attainment
Basophil % of granulocytes
BMI-adjusted waist-hip ratio
Genetic disorder
Sitting height
Monocyte % of leukocytes
High density lipoprotein cholesterol
Hemoglobin
Granulocyte % of myeloid white cells
F
AoU: PACC1 variant association with septicemia
P = 0.023
0.0
0.5
1.0
1.5
2.0
Odds ratio

493

494 **Fig. 1. *PACC1* expression is enriched in human mononuclear phagocytes, particularly tissue**
495 **macrophages, and *PACC1* variants are implicated in myeloid cell-mediated immunity.**
496 **A-D** Single-cell RNA sequencing (scRNA-seq) data from the Human Protein Atlas (HPA) or bulk RNA-
497 seq data from the ImmGen Immune Cell Atlas (ICA), as indicated. Curated cell types along the x-axis
498 contain *superimposed* (not stacked) data from cells that were clustered and annotated (HPA), or sorted
499 (ICA), such that each horizontal line on the bar graphs represents the gene expression for an individual
500 cell type/cluster. HPA data are normalized transcripts per million (nTPM), corresponding to means of
501 different individual samples from each cell type. ICA data are mean normalized counts from different
502 individual samples. Red arrows/boxes indicate cells of interest within each panel (e.g., immune cells,
503 mononuclear phagocytes, or macrophages). (**A**) *PACC1* expression in somatic human cell types from
504 the HPA. (**B**) *PACC1* expression in blood immune cells from the HPA. (**C**) *PACC1* expression in blood
505 immune cells from the ICA. (**D**) *PACC1* expression in all 19 somatic tissues from the HPA wherein tissue
506 macrophages were annotated. Cell clusters are broadly curated in combined columns (e.g., epithelial
507 cells, endothelial cells), while immune cell clusters are resolved in separate columns (e.g., macrophages,
508 granulocytes). Data represent $\log_{10}$(mean nTPM + 1) corresponding to means of different clusters from
509 each cell type. Dots indicate tissue macrophage-containing cell types that rank first (white) and/or second
510 (black) in terms of *PACC1* expression amongst all cell types within each tissue. (**E**) Heatmap ranking
511 showing the most well-evidenced *PACC1* genetic variant associations across all phenotypes, according
512 to the Open Targets Platform for genome-wide association studies (GWAS), ranked by "association
513 scores" which synthesize evidence across databases (e.g., OT Genetics, NIH ClinVar, Gene Burden).
514 Red arrows/boxes indicate *PACC1* variant associations with phenotypes of interest (i.e., myeloid cell-
515 related phenotypes). (**F**) Forest plot showing association between gene-level predicted loss-of-function
516 variant burden (low, rare and ultra rare, minor allele frequency <1%) in *PACC1* with septicemia phecode
517 in the AoU dataset. The plot shows burden test P-value, odds ratio, and 95% confidence interval.

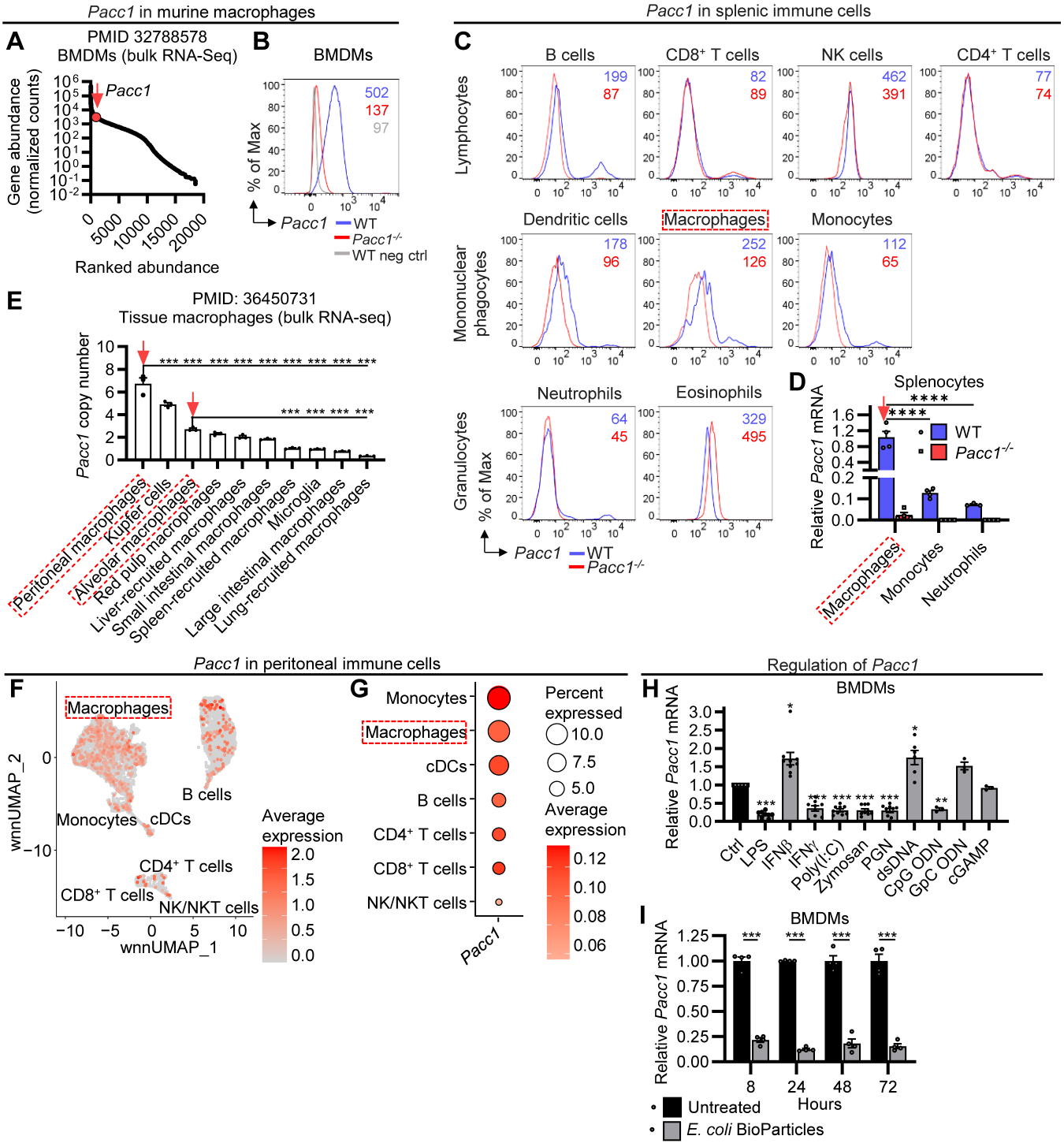
Pacc1 in murine macrophages
A
PMID 32788578
BMDMs (bulk RNA-Seq)
Gene abundance (normalized counts)
Pacc1
Ranked abundance
B
BMDMs
% of Max
502
137
97
Pacc1
WT
Pacc1-/-
WT neg ctrl
E
PMID: 36450731
Tissue macrophages (bulk RNA-seq)
Pacc1 copy number
Peritoneal macrophages
Kupffer cells
Alveolar macrophages
Red pulp macrophages
Liver-recruited macrophages
Small intestinal macrophages
Spleen-recruited macrophages
Microglia
Large intestinal macrophages
Lung-recruited macrophages
Pacc1 in splenic immune cells
C
Lymphocytes
B cells
CD8+ T cells
NK cells
CD4+ T cells
Mononuclear phagocytes
Dendritic cells
Macrophages
Monocytes
Granulocytes
Neutrophils
Eosinophils
% of Max
Pacc1
WT
Pacc1-/-
D
Splenocytes
Relative Pacc1 mRNA
WT
Pacc1-/-
Macrophages
Monocytes
Neutrophils
Pacc1 in peritoneal immune cells
F
Macrophages
B cells
Monocytes
cDCs
CD4+ T cells
CD8+ T cells
NK/NKT cells
wnnUMAP_1
wnnUMAP_2
Average expression
G
Monocytes
Macrophages
cDCs
B cells
CD4+ T cells
CD8+ T cells
NK/NKT cells
Pacc1
Percent expressed
Average expression
Regulation of Pacc1
H
BMDMs
Relative Pacc1 mRNA
Ctrl
LPS
IFNβ
IFNγ
Poly(I:C)
Zymosan
PGN
dsDNA
CpG ODN
GpC ODN
cGAMP
I
BMDMs
Relative Pacc1 mRNA
Hours
Untreated
E. coli BioParticles

518

519 **Fig. 2. *Pacc1* expression is highly expressed in murine macrophages and other mononuclear**
520 **phagocytes.**

521 (**A**) Ranked gene expression of bulk RNA sequencing (bulk RNA-seq) data of bone marrow-derived
522 macrophages (BMDMs) isolated *ex vivo* from wildtype (WT) mice. Data reanalyzed from our previous
523 study *(11)*. *Pacc1* expression shown in red in the top 5%. (**B-C**) *Pacc1* mRNA fluorescence by RNA
524 PrimeFlow staining in splenocytes from WT and *Pacc1* knockout (*Pacc1*$^{-/-}$) mice. Geometric mean
525 fluorescence intensities (MFIs) are indicated in the upper right. (**B**) Representative flow cytometric
526 histograms of *Pacc1* expression in resting bone marrow-derived macrophages (BMDMs). Neg ctrl
527 indicates no target probe. (**C**) Representative flow cytometric histograms of *Pacc1* expression in
528 splenocytes. (**D**) *Pacc1* expression in selected FACSorted splenocyte myeloid cell populations (live
529 CD11b^{+}F4/80^{+} macrophages, CD11b^{+}Ly6C^{+}Ly6G^{-} monocytes, and CD11b^{+}Ly6C^{+}Ly6G^{+} neutrophils) by
530 RT-qPCR normalized to WT macrophage expression. (**E**) *Pacc1* copy number in bulk RNA-seq data from
531 tissue macrophages isolated from WT mice. Data reanalyzed from Qie *et al.* (49). (**F-G**) *Pacc1* expression
532 by single-nucleus RNA sequencing of peritoneal cells from WT mice. (**F**) *Pacc1* expression in annotated
533 immune cell clusters visualized on the weight-nearest neighbor uniform manifold approximation and
534 projection (wnnUMAP) plot. (**G**) Dot plot of *Pacc1* expression from **F**. (**H**) *Pacc1* expression in stimulated
535 WT BMDMs analyzed by RT-qPCR, normalized to untreated control. In brief, BMDMs were stimulated
536 for 24 h with various stimuli corresponding to inflammatory/infectious insults, including lipopolysaccharide
537 (LPS), interferon-beta (IFN-β), interferon-gamma (IFN-ɣ), polyinosinic:polycytidylic acid (poly I:C),
538 zymosan, peptidoglycan (PGN), double-stranded DNA (dsDNA), CpG oligodeoxynucleotides (ODN),
539 GpC ODN, or cyclic guanosine monophosphate–adenosine monophosphate (cGAMP). (**I**) *Pacc1*
540 expression in BMDMs stimulated with inactivated *E. coli* Bioparticles analyzed by RT-qPCR, normalized
541 to untreated control at each time point. For **B**-**D**, **H**, **I**, data represent ≥2 independent experiments. For **D**,
542 **E**, **H**, **I**, data show one symbol per mouse, mean±SEM, *P<0.05, **P<0.01, ***P<0.001,
543 ****P<0.0001,one-way ANOVA with Tukey (**D**), one-way ANOVA with Sidak (**E**, **I**), two-way ANOVA with
544 Tukey (**D**), or one-way ANOVA with Dunett comparing each to unstimulated control (**H**). For **C**-**G**, red

545 arrows/boxes indicate cells of interest (i.e., macrophage populations).

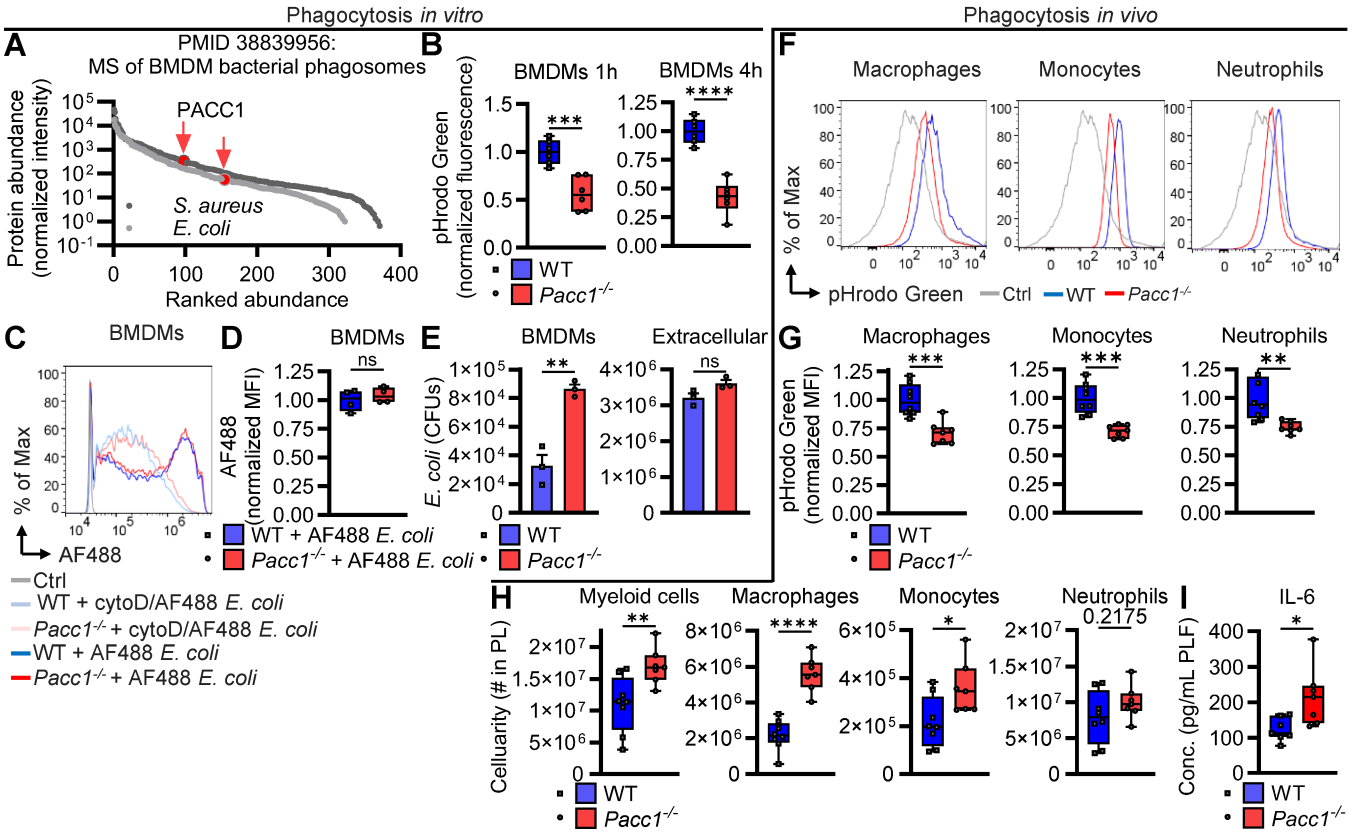
Phagocytosis in vitro
Phagocytosis in vivo
A
PMID 38839956:
MS of BMDM bacterial phagosomes
Protein abundance (normalized intensity)
PACC1
S. aureus
E. coli
Ranked abundance
B
BMDMs 1h
BMDMs 4h
pHrodo Green (normalized fluorescence)
WT
Pacc1-/-
C
BMDMs
% of Max
AF488
Ctrl
WT + cytoD/AF488 E. coli
Pacc1-/- + cytoD/AF488 E. coli
WT + AF488 E. coli
Pacc1-/- + AF488 E. coli
D
BMDMs
AF488 (normalized MFI)
ns
E
BMDMs
Extracellular
E. coli (CFUs)
F
Macrophages
Monocytes
Neutrophils
% of Max
pHrodo Green
G
pHrodo Green (normalized MFI)
H
Myeloid cells
Macrophages
Monocytes
Neutrophils
0.2175
Celluarity (# in PL)
I
IL-6
Conc. (pg/mL PLF)

546

547 **Fig. 3. *Pacc1*$^{-/-}$ mice have defective development of the acidifying phagolysosome.**

548 (**A**) Ranked protein abundance from mass spectrometry (MS) data of the phagosomes of bone-marrow-
549 derived macrophages (BMDMs) stimulated with bacteria. Data reanalyzed from Li *et al.* (51). In brief,
550 BMDMs were stimulated with ascorbate peroxidase (APEX)-modified inactivated bacteria followed by
551 APEX-mediated proximity ligation, and subsequently MS, to identify bacterial phagosomal proteins.
552 PACC1 is highlighted in red. (**B**) Wildtype (WT) and *Pacc1*$^{-/-}$ BMDMs were treated with 330 µg/mL acid-
553 sensitive pHrodo Green *E. coli* BioParticles for the indicated time points. Fluorescence was measured by
554 plate-reader and normalized to WT for each time point to assay development of phagolysosomal
555 acidification. (**C-D)** WT and *Pacc1*$^{-/-}$ BMDMs were treated with acid-insensitive Alexa Fluor (AF)488 *E.*
556 *coli* BioParticles. After 1 h, AF488 geometric mean fluorescence intensity (MFI) was measured by flow
557 cytometry to assay phagocytic uptake. (**C**) Representative flow cytometric histograms of BMDMs are
558 shown. CytoD indicates negative control cells pre-treated with actin inhibitor, cytochalasin D, for 1 hour
559 at 10µM to limit phagocytic uptake. Ctrl indicates negative control WT cells treated with inactivated *E. coli*
560 without fluorescent conjugation. (**D**) MFI quantifications from panel **C**, normalized to WT. (**E**) Colony-
561 forming unit (CFU) counts from WT and *Pacc1*$^{-/-}$ BMDMs infected with pathogenic *E. coli* serotype
562 O6:K2:H1 at an MOI of 5 for 2 h. CFUs in macrophage lysates and extracellular supernatants via serially
563 diluted plated cultures to assay bacterial killing capacity. (**F-I**) WT and *Pacc1*$^{-/-}$ mice were injected i.p.
564 with 100 µg pHrodo Green *E. coli* BioParticles. After 24 h, cellularity and pHrodo Green MFI were
565 measured by flow cytometry to assay development of phagolysosomal acidification from peritoneal
566 lavage cells. (**F**) Representative flow cytometric histograms of live CD11b^{+}Ly6C$^{-/lo}$F4/80^{+} macrophages,
567 CD11b^{+}Ly6C^{hi}Ly6G^{-} monocytes, and CD11b^{+}Ly6C^{+}Ly6G^{+} neutrophils are shown. Ctrl indicates
568 fluorescence of total live cells from an unstimulated WT mouse. (**G**) MFI quantifications from panel **F**,
569 normalized to WT. (**H**) Cell numbers from the peritoneal lavage (PL) of the same *E. coli* experiments
570 above, including total live CD11b^{+} myeloid cells by flow cytometry. (**I**) IL-6 concentration in peritoneal
571 lavage fluid (PLF) by ELISA from the same *E. coli* experiments above. For **B-I**, data represent ≥2
572 independent experiments. For **B**, **D**, **E**, **G-I**, data show one symbol per mouse. Bar graphs depict

573 mean±SEM, and box plots show median and interquartile range with whiskers extended to the minimum

574 and maximum. *P<0.05, **P<0.01, ***P<0.001, ****P<0.0001, ns=not significant, Student's t-test.

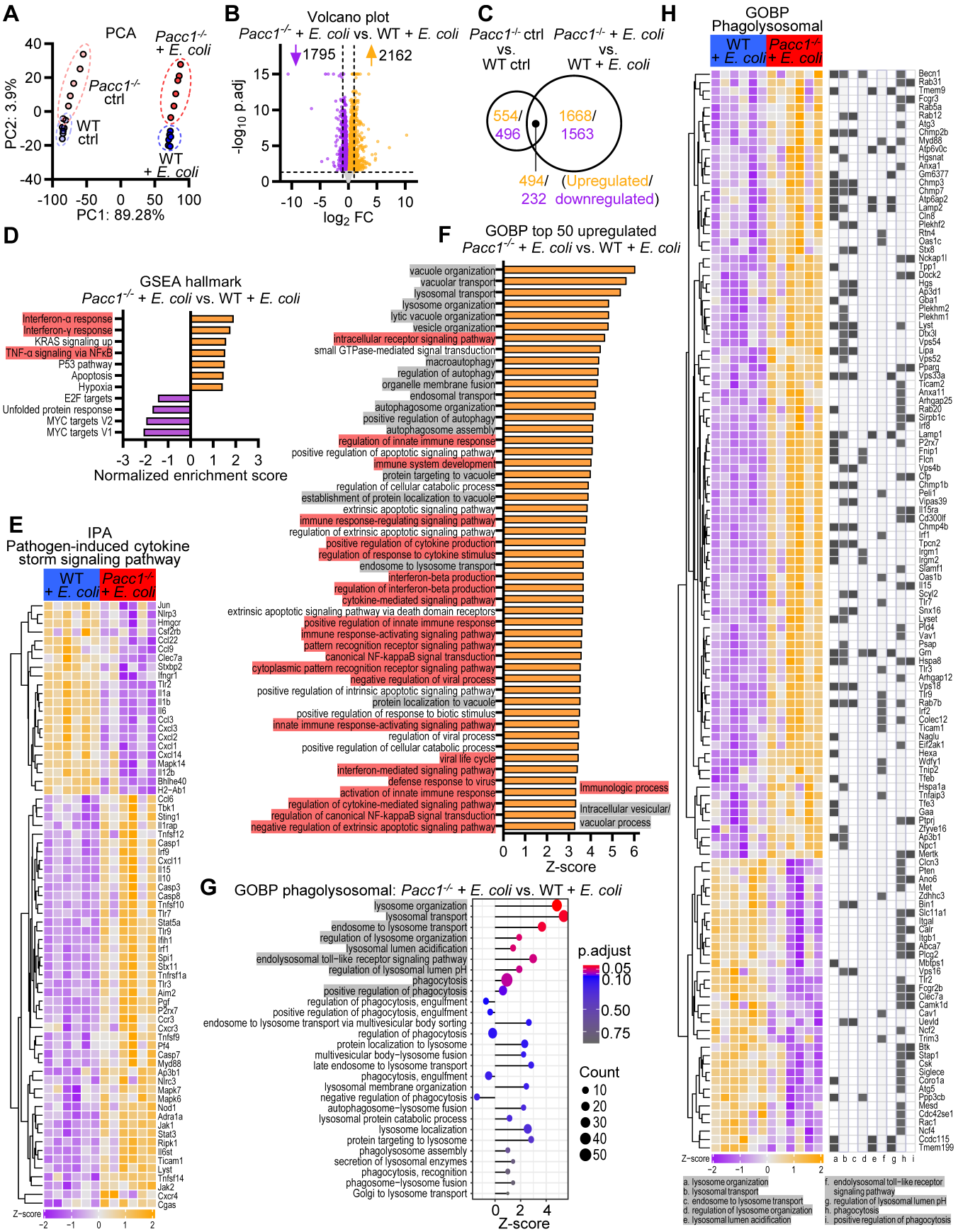
A
PCA
Pacc1-/- + E. coli
Pacc1-/- ctrl
WT ctrl
WT + E. coli
PC2: 3.9%
PC1: 89.28%
B
Volcano plot
Pacc1-/- + E. coli vs. WT + E. coli
1795
2162
-log10 p.adj
log2 FC
C
Pacc1-/- ctrl vs. WT ctrl
Pacc1-/- + E. coli vs. WT + E. coli
554/ 496
1668/ 1563
494/ 232
(Upregulated/ downregulated)
D
GSEA hallmark
Pacc1-/- + E. coli vs. WT + E. coli
Interferon-α response
Interferon-γ response
KRAS signaling up
TNF-α signaling via NFκB
P53 pathway
Apoptosis
Hypoxia
E2F targets
Unfolded protein response
MYC targets V2
MYC targets V1
Normalized enrichment score
E
IPA
Pathogen-induced cytokine storm signaling pathway
WT + E. coli
Pacc1-/- + E. coli
Z-score
F
GOBP top 50 upregulated
Pacc1-/- + E. coli vs. WT + E. coli
vacuole organization
vacuolar transport
lysosomal transport
lysosome organization
lytic vacuole organization
vesicle organization
intracellular receptor signaling pathway
small GTPase-mediated signal transduction
macroautophagy
regulation of autophagy
organelle membrane fusion
endosomal transport
autophagosome organization
positive regulation of autophagy
autophagosome assembly
regulation of innate immune response
positive regulation of apoptotic signaling pathway
immune system development
protein targeting to vacuole
regulation of cellular catabolic process
establishment of protein localization to vacuole
extrinsic apoptotic signaling pathway
immune response-regulating signaling pathway
regulation of extrinsic apoptotic signaling pathway
positive regulation of cytokine production
regulation of response to cytokine stimulus
endosome to lysosome transport
interferon-beta production
regulation of interferon-beta production
cytokine-mediated signaling pathway
extrinsic apoptotic signaling pathway via death domain receptors
positive regulation of innate immune response
immune response-activating signaling pathway
pattern recognition receptor signaling pathway
canonical NF-kappaB signal transduction
cytoplasmic pattern recognition receptor signaling pathway
negative regulation of viral process
positive regulation of intrinsic apoptotic signaling pathway
protein localization to vacuole
positive regulation of response to biotic stimulus
innate immune response-activating signaling pathway
regulation of viral process
positive regulation of cellular catabolic process
viral life cycle
interferon-mediated signaling pathway
defense response to virus
activation of innate immune response
regulation of cytokine-mediated signaling pathway
regulation of canonical NF-kappaB signal transduction
negative regulation of extrinsic apoptotic signaling pathway
Immunologic process
Intracellular vesicular/ vacuolar process
Z-score
G
GOBP phagolysosomal: Pacc1-/- + E. coli vs. WT + E. coli
lysosome organization
lysosomal transport
endosome to lysosome transport
regulation of lysosome organization
lysosomal lumen acidification
endolysosomal toll-like receptor signaling pathway
regulation of lysosomal lumen pH
phagocytosis
positive regulation of phagocytosis
regulation of phagocytosis, engulfment
positive regulation of phagocytosis, engulfment
endosome to lysosome transport via multivesicular body sorting
regulation of phagocytosis
protein localization to lysosome
multivesicular body−lysosome fusion
late endosome to lysosome transport
phagocytosis, engulfment
lysosomal membrane organization
negative regulation of phagocytosis
autophagosome−lysosome fusion
lysosomal protein catabolic process
lysosome localization
protein targeting to lysosome
phagolysosome assembly
secretion of lysosomal enzymes
phagocytosis, recognition
phagosome−lysosome fusion
Golgi to lysosome transport
p.adjust
0.05
0.10
0.50
0.75
Count
10
20
30
40
50
Z-score
H
GOBP Phagolysosomal
WT + E. coli
Pacc1-/- + E. coli
Z-score
a. lysosome organization
b. lysosomal transport
c. endosome to lysosome transport
d. regulation of lysosome organization
e. lysosomal lumen acidification
f. endolysosomal toll−like receptor signaling pathway
g. regulation of lysosomal lumen pH
h. phagocytosis
i. positive regulation of phagocytosis

575

576 **Fig. 4. Transcriptomic profiling of dysregulated immunologic and phagolysosomal pathways in**
577 **bone marrow-derived macrophages (BMDMs) from *Pacc1*$^{-/-}$ mice and wildtype mice stimulated**
578 **with *E. coli* Bioparticles.**

579 Wildtype (WT) and *Pacc1*$^{-/-}$ BMDMs were stimulated with *E. coli* BioParticles at 100 µg/mL or left as
580 unstimulated controls (ctrl) for 12 h and subjected to bulk RNA sequencing (n=6 mice/group). (**A**) Principal
581 component analysis (PCA) plot of the top 5000 variable genes after variance-stabilizing transformation
582 of sequencing counts, displaying *E. coli*-dependent and genotype-dependent clusters. (**B**) Volcano plot
583 of differentially expressed genes (DEGs) in *Pacc1*$^{-/-}$ vs. WT BMDMs following *E. coli* stimulation. Dotted
584 lines indicate adj. P=0.05 and absolute $\log_2$ fold change (FC)=1; values for -$\log_{10}$ adj. P>15 were set=15
585 for visualization. (**C**) Venn diagram showing common and specific significant DEGs in *Pacc1*$^{-/-}$ vs. WT
586 BMDMs with or without *E. coli*. (**D**) Bar plot showing hallmark gene set enrichment analysis (GSEA) in
587 *Pacc1*$^{-/-}$ vs. WT BMDMs with *E. coli*. Immunologic pathways in red. (**E**) Heatmap of significant DEGs
588 enriched in "Pathogen Induced Cytokine Storm Signaling Pathway" from Ingenuity Pathway Analysis
589 (IPA) in *Pacc1*$^{-/-}$ vs. WT BMDMs with *E. coli*. Normalized expression values. (**F**) Bar plot showing top 50
590 significant (adj. P<0.1) positively enriched gene ontology biological processes (GOBPs) in *Pacc1*$^{-/-}$ vs.
591 WT BMDMs with *E. coli*. Immunologic pathways are in red, intracellular vesicular/vacuolar pathways in
592 gray. (**G**) Lollipop plot of manually curated phagolysosomal GOBPs showing both enriched (adj. P<0.1)
593 and non-enriched in *Pacc1*$^{-/-}$ vs. WT BMDMs with *E. coli*. (**H**) Heatmap of significant DEGs within enriched
594 (adj. P<0.1) phagolysosomal GOBPs from panel **G** in *Pacc1*$^{-/-}$ vs. WT BMDMs with *E. coli*. Genes
595 enriched within each GOBP are indicated by shaded squares. Heatmaps show normalized expression
596 values with Z-score from -2/purple to +2/orange and significance at adj. P<0.05. See also ***SI Appendix,***
597 **Datasets 1–4**.

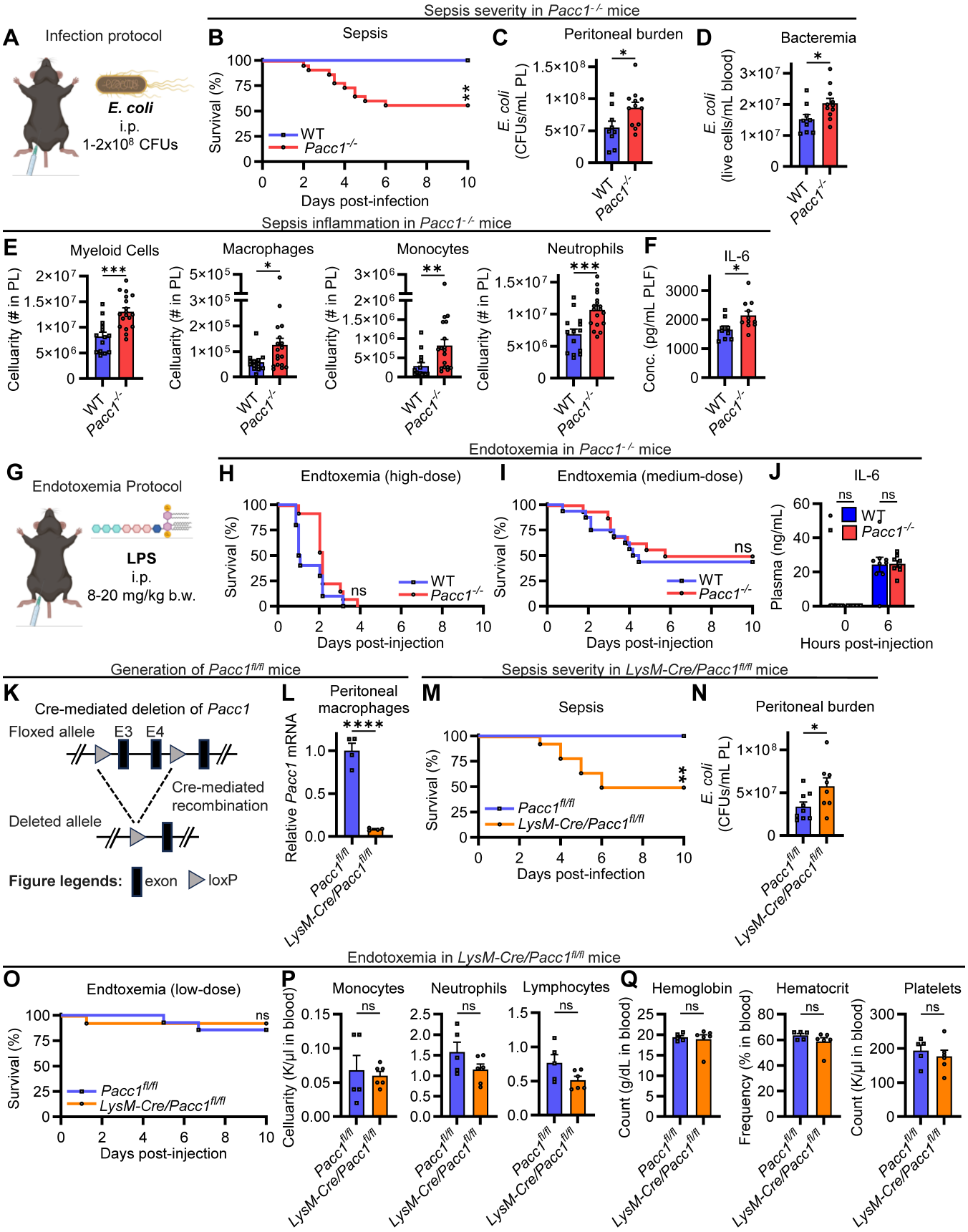
Sepsis severity in Pacc1-/- mice
A
Infection protocol
E. coli
i.p.
1-2x10^8 CFUs
B
Sepsis
Survival (%)
WT
Pacc1-/-
Days post-infection
C
Peritoneal burden
E. coli (CFUs/mL PL)
D
Bacteremia
E. coli (live cells/mL blood)
Sepsis inflammation in Pacc1-/- mice
E
Myeloid Cells
Macrophages
Monocytes
Neutrophils
Celluarity (# in PL)
F
IL-6
Conc. (pg/mL PLF)
Endotoxemia in Pacc1-/- mice
G
Endotoxemia Protocol
LPS
i.p.
8-20 mg/kg b.w.
H
Endtoxemia (high-dose)
I
Endtoxemia (medium-dose)
J
IL-6
Plasma (ng/mL)
Hours post-injection
Generation of Pacc1fl/fl mice
K
Cre-mediated deletion of Pacc1
Floxed allele
E3
E4
Cre-mediated recombination
Deleted allele
Figure legends:
exon
loxP
L
Peritoneal macrophages
Relative Pacc1 mRNA
Pacc1fl/fl
LysM-Cre/Pacc1fl/fl
Sepsis severity in LysM-Cre/Pacc1fl/fl mice
M
Sepsis
N
Peritoneal burden
Endotoxemia in LysM-Cre/Pacc1fl/fl mice
O
Endtoxemia (low-dose)
P
Monocytes
Neutrophils
Lymphocytes
Celluarity (K/µl in blood)
Q
Hemoglobin
Count (g/dL in blood)
Hematocrit
Frequency (% in blood)
Platelets
Count (K/µl in blood)

598

599 **Fig. 5. Global and myeloid cell conditional *Pacc1* deletion confers susceptibility to *E. coli* sepsis.**
600 (**A**) Schematic showing sepsis infection. Wildtype (WT) and *Pacc1*$^{-/-}$ mice were given 1-2x10^8 colony-
601 forming units (CFUs) of *Escherichia (E). coli* intraperitoneally (i.p.). Peritoneal lavage (PL) and blood were
602 collected after 6 or 24 h, or survival was monitored, as indicated. (**B**) Sepsis survival (n=17-22
603 mice/group, pooled from 3 independent experiments). (**C**) CFUs in PL after 6 h assayed by serially diluted
604 plated cultures. (**D**) Number of live bacteria in blood after 24 h by flow cytometry. (**E**) Myeloid cell numbers
605 in PL after 24 h by flow cytometry. (**F**) IL-6 in PL fluid (PLF) after 6 h by ELISA. (**G**) Schematic showing
606 endotoxemia induction. Mice were given *E. coli*-derived lipopolysaccharide (LPS) i.p. to induce
607 phagocytosis-independent endotoxemia. (**H**) Endotoxemia survival with high-dose (20 mg/kg body weight
608 [b.w.]) LPS (n=10-13 mice/group) and (**I**) medium-dose (10 mg/kg b.w.) LPS (n=16 mice/group, 2 pooled
609 experiments). (**J**) IL-6 in plasma after low-dose endotoxemia as in panel H by ELISA. (**K**) Schematic
610 showing generation of *Pacc1*-floxed mice and Cre-mediated deletion. In brief, LoxP sites flanking exons
611 3/4 of the *Pacc1* were inserted using CRISPR/Cas9 in WT mice, such that their Cre-mediated deletion
612 eliminates productive *Pacc1* expression. (**L**) *Pacc1* expression loss in live CD11b$^+$F4/80$^+$ peritoneal
613 macrophages from *LysM-Cre/Pacc1*$^{fl/fl}$ mice by qRT-PCR. *Pacc1*-floxed (*Pacc1*$^{fl/fl}$) and *LysM-Cre* mice
614 were crossed for targeted deletion of *Pacc1* in myeloid cells, and macrophages were FACSorted from
615 the PL of naïve mice. (**M**) Sepsis survival following *E. coli* infection as in A (n=11-14 mice/group, 2 pooled
616 experiments). (**N**) CFUs in PL after 6 h by serially diluted plated cultures. (**O**) Endotoxemia survival with
617 low-dose (8 mg/kg b.w.) LPS (n=14 mice/group). Parameters determined by blood analyzer in mice with
618 low-dose endotoxemia after 24 h, including (**P**) immune cell counts and (**Q**) blood parameters. Data
619 represent ≥2 independent experiments and show one symbol per mouse, mean±SEM, *P<0.05,
620 **P<0.01, ***P<0.001, ns=not significant, Student's t-test (**C**-**F, J**, **L**, **N**, **P**, **Q**), or Mantel-Cox log-rank test
621 (**B**, **H**, **I**, **M**, **O**).

References

1. K. E. Rudd *et al.*, Global, regional, and national sepsis incidence and mortality, 1990-2017: analysis for the Global Burden of Disease Study. *Lancet* **395**, 200-211 (2020).
2. C. J. Paoli, M. A. Reynolds, M. Sinha, M. Gitlin, E. Crouser, Epidemiology and Costs of Sepsis in the United States-An Analysis Based on Timing of Diagnosis and Severity Level. *Crit Care Med* **46**, 1889-1897 (2018).
3. C. M. Torio, B. J. Moore, "National Inpatient Hospital Costs: The Most Expensive Conditions by Payer, 2013" in Healthcare Cost and Utilization Project (HCUP) Statistical Briefs. (Agency for Healthcare Research and Quality (US), Rockville (MD), 2006).
4. C. Rhee *et al.*, Prevalence, Underlying Causes, and Preventability of Sepsis-Associated Mortality in US Acute Care Hospitals. *JAMA Netw Open* **2**, e187571 (2019).
5. L. J. Quinton, A. J. Walkey, J. P. Mizgerd, Integrative Physiology of Pneumonia. *Physiol Rev* **98**, 1417-1464 (2018).
6. Anonymous, Global burden of bacterial antimicrobial resistance 1990-2021: a systematic analysis with forecasts to 2050. *Lancet* 10.1016/s0140-6736(24)01867-1 (2024).
7. E. Karakike *et al.*, Coronavirus Disease 2019 as Cause of Viral Sepsis: A Systematic Review and Meta-Analysis. *Crit Care Med* **49**, 2042-2057 (2021).
8. M. Bonten *et al.*, Epidemiology of Escherichia coli Bacteremia: A Systematic Literature Review. *Clin Infect Dis* **72**, 1211-1219 (2021).
9. Anonymous, Global mortality associated with 33 bacterial pathogens in 2019: a systematic analysis for the Global Burden of Disease Study 2019. *Lancet* **400**, 2221-2248 (2022).
10. M. Bosmann *et al.*, Interruption of macrophage-derived IL-27(p28) production by IL-10 during sepsis requires STAT3 but not SOCS3. *J Immunol* **193**, 5668-5677 (2014).
11. J. Roewe *et al.*, Bacterial polyphosphates interfere with the innate host defense to infection. *Nat Commun* **11**, 4035 (2020).
12. M. Bosmann, N. F. Russkamp, P. A. Ward, Fingerprinting of the TLR4-induced acute inflammatory response. *Exp Mol Pathol* **93**, 319-323 (2012).
13. M. Bosmann *et al.*, CD11c+ alveolar macrophages are a source of IL-23 during lipopolysaccharide-induced acute lung injury. *Shock* **39**, 447-452 (2013).
14. S. H. E. Kaufmann, A. Dorhoi, R. S. Hotchkiss, R. Bartenschlager, Host-directed therapies for bacterial and viral infections. *Nat Rev Drug Discov* **17**, 35-56 (2018).
15. M. Bosmann, P. A. Ward, The inflammatory response in sepsis. *Trends Immunol* **34**, 129-136 (2013).
16. E. Mass, F. Nimmerjahn, K. Kierdorf, A. Schlitzer, Tissue-specific macrophages: how they develop and choreograph tissue biology. *Nature Reviews Immunology* **23**, 563-579 (2023).
17. A. M. Pauwels, M. Trost, R. Beyaert, E. Hoffmann, Patterns, Receptors, and Signals: Regulation of Phagosome Maturation. *Trends Immunol* **38**, 407-422 (2017).
18. E. Uribe-Querol, C. Rosales, Phagocytosis: Our Current Understanding of a Universal Biological Process. *Front Immunol* **11**, 1066 (2020).
19. T. J. Jentsch, M. Pusch, CLC Chloride Channels and Transporters: Structure, Function, Physiology, and Disease. *Physiol Rev* **98**, 1493-1590 (2018).
20. T. Stauber, T. J. Jentsch, Chloride in vesicular trafficking and function. *Annu Rev Physiol* **75**, 453-477 (2013).
21. J. Yang *et al.*, PAC, an evolutionarily conserved membrane protein, is a proton-activated chloride channel. *Science* **364**, 395-399 (2019).
22. F. Ullrich *et al.*, Identification of TMEM206 proteins as pore of PAORAC/ASOR acid-sensitive chloride channels. *Elife* **8** (2019).
23. S. Lambert, J. Oberwinkler, Characterization of a proton-activated, outwardly rectifying anion channel. *J Physiol* **567**, 191-213 (2005).

24. C. Auzanneau, V. Thoreau, A. Kitzis, F. Becq, A Novel voltage-dependent chloride current activated by extracellular acidic pH in cultured rat Sertoli cells. *J Biol Chem* **278**, 19230-19236 (2003).
25. H. Y. Wang, T. Shimizu, T. Numata, Y. Okada, Role of acid-sensitive outwardly rectifying anion channels in acidosis-induced cell death in human epithelial cells. *Pflugers Arch* **454**, 223-233 (2007).
26. Z. Ruan, J. Osei-Owusu, J. Du, Z. Qiu, W. Lü, Structures and pH-sensing mechanism of the proton-activated chloride channel. *Nature* **588**, 350-354 (2020).
27. J. Osei-Owusu *et al.*, Molecular determinants of pH sensing in the proton-activated chloride channel. *Proc Natl Acad Sci U S A* **119**, e2200727119 (2022).
28. C. Wang, M. M. Polovitskaya, B. D. Delgado, T. J. Jentsch, S. B. Long, Gating choreography and mechanism of the human proton-activated chloride channel ASOR. *Sci Adv* **8**, eabm3942 (2022).
29. Z. Deng *et al.*, Cryo-EM structure of a proton-activated chloride channel TMEM206. *Sci Adv* **7** (2021).
30. J. Osei-Owusu, J. Yang, M. Del Carmen Vitery, M. Tian, Z. Qiu, PAC proton-activated chloride channel contributes to acid-induced cell death in primary rat cortical neurons. *Channels (Austin)* **14**, 53-58 (2020).
31. X. M. Zha, Z. G. Xiong, R. P. Simon, pH and proton-sensitive receptors in brain ischemia. *J Cereb Blood Flow Metab* **42**, 1349-1363 (2022).
32. P. Xue *et al.*, Proton-Activated Chloride Channel Increases Endplate Porosity and Pain in a Mouse Spinal Degeneration Model. *J Clin Invest* 10.1172/jci168155 (2024).
33. J. E. DiCiccio, B. E. Steinberg, Lysosomal pH and analysis of the counter ion pathways that support acidification. *J Gen Physiol* **137**, 385-390 (2011).
34. J. Osei-Owusu *et al.*, Proton-activated chloride channel PAC regulates endosomal acidification and transferrin receptor-mediated endocytosis. *Cell Rep* **34**, 108683 (2021).
35. M. Zeziulia, S. Blin, F. W. Schmitt, M. Lehmann, T. J. Jentsch, Proton-gated anion transport governs macropinosome shrinkage. *Nat Cell Biol* **24**, 885-895 (2022).
36. K. H. Chen *et al.*, Loss of the proton-activated chloride channel in neurons impairs AMPA receptor endocytosis and LTD via endosomal hyper-acidification. *Cell Rep* **44**, 115302 (2025).
37. N. Koylass *et al.*, The Proton-Activated Chloride Channel Inhibits SARS-CoV-2 Spike Protein-Mediated Viral Entry Through the Endosomal Pathway. *J Cell Physiol* **240**, e70063 (2025).
38. M. Karlsson *et al.*, A single-cell type transcriptomics map of human tissues. Further details available at: https://www.proteinatlas.org/about/assays+annotation#normalization_rna. *Sci Adv* **7** (2021).
39. T. S. Heng, M. W. Painter, The Immunological Genome Project: networks of gene expression in immune cells. *Nat Immunol* **9**, 1091-1094 (2008).
40. Y. J. Jung, W. S. Chung, Phagocytic Roles of Glial Cells in Healthy and Diseased Brains. *Biomol Ther (Seoul)* **26**, 350-357 (2018).
41. A. J. Byrne, S. A. Mathie, L. G. Gregory, C. M. Lloyd, Pulmonary macrophages: key players in the innate defence of the airways. *Thorax* **70**, 1189-1196 (2015).
42. A. Madhvi, H. Mishra, G. R. Leisching, P. Z. Mahlobo, B. Baker, Comparison of human monocyte derived macrophages and THP1-like macrophages as in vitro models for M. tuberculosis infection. *Comp Immunol Microbiol Infect Dis* **67**, 101355 (2019).
43. C. Klijn *et al.*, A comprehensive transcriptional portrait of human cancer cell lines. *Nat Biotechnol* **33**, 306-312 (2015).
44. D. Ochoa *et al.*, The next-generation Open Targets Platform: reimagined, redesigned, rebuilt. *Nucleic Acids Res* **51**, D1353-d1359 (2023).
45. S. J. Jurgens *et al.*, Rare coding variant analysis for human diseases across biobanks and ancestries. *Nat Genet* **56**, 1811-1820 (2024).

720 46. C. Bycroft *et al.*, The UK Biobank resource with deep phenotyping and genomic data. *Nature* **562**,
721 203-209 (2018).
722 47. S. F. Pastore *et al.*, Biallelic inheritance in a single Pakistani family with intellectual disability
723 implicates new candidate gene RDH14. *Sci Rep* **11**, 23113 (2021).
724 48. C. Lai, D. Stepniak, L. Sias, C. Funatake, A sensitive flow cytometric method for multi-parametric
725 analysis of microRNA, messenger RNA and protein in single cells. *Methods* **134-135**, 136-148
726 (2018).
727 49. J. Qie *et al.*, Integrated proteomic and transcriptomic landscape of macrophages in mouse
728 tissues. *Nature Communications* **13**, 7389 (2022).
729 50. S. Lykke-Andersen, T. H. Jensen, Nonsense-mediated mRNA decay: an intricate machinery that
730 shapes transcriptomes. *Nature Reviews Molecular Cell Biology* **16**, 665-677 (2015).
731 51. K. Li *et al.*, Profiling phagosome proteins identifies PD-L1 as a fungal-binding receptor. *Nature*
732 **630**, 736-743 (2024).
733 52. A. Neaga, J. Lefor, K. E. Lich, S. F. Liparoto, Y. Q. Xiao, Development and validation of a flow
734 cytometric method to evaluate phagocytosis of pHrodo™ BioParticles® by granulocytes in
735 multiple species. *J Immunol Methods* **390**, 9-17 (2013).
736 53. B. Lindner, T. Burkard, M. Schuler, Phagocytosis assays with different pH-sensitive fluorescent
737 particles and various readouts. *Biotechniques* **68**, 245-250 (2020).
738 54. C. Lambert *et al.*, Cytochalasans and Their Impact on Actin Filament Remodeling. *Biomolecules*
739 **13** (2023).
740 55. I. Rusinova *et al.*, Interferome v2.0: an updated database of annotated interferon-regulated genes.
741 *Nucleic Acids Res* **41**, D1040-1046 (2013).
742 56. M. Dudek *et al.*, Lung epithelium and myeloid cells cooperate to clear acute pneumococcal
743 infection. *Mucosal Immunol* **9**, 1288-1302 (2016).
744 57. J. C. Gomez *et al.*, Mechanisms of interferon-γ production by neutrophils and its function during
745 Streptococcus pneumoniae pneumonia. *Am J Respir Cell Mol Biol* **52**, 349-364 (2015).
746 58. C. L. Abram, G. L. Roberge, Y. Hu, C. A. Lowell, Comparative analysis of the efficiency and
747 specificity of myeloid-Cre deleting strains using ROSA-EYFP reporter mice. *J Immunol Methods*
748 **408**, 89-100 (2014).
749 59. H. Y. Cheng *et al.*, Proton-activated chloride channel governs phagosome-mediated antibacterial
750 immunity in peritoneal macrophages. *J Exp Med* **222** (2025).
751 60. B. E. Steinberg *et al.*, A cation counterflux supports lysosomal acidification. *J Cell Biol* **189**, 1171-
752 1186 (2010).
753 61. S. Weinert *et al.*, Uncoupling endosomal CLC chloride/proton exchange causes severe
754 neurodegeneration. *Embo j* **39**, e103358 (2020).
755 62. A. Lukasiak, M. Zajac, The Distribution and Role of the CFTR Protein in the Intracellular
756 Compartments. *Membranes* **11**, 804 (2021).
757 63. A. Meoli *et al.*, Impact of CFTR Modulators on the Impaired Function of Phagocytes in Cystic
758 Fibrosis Lung Disease. *Int J Mol Sci* **23** (2022).
759 64. A. Badr *et al.*, CFTR Modulators Restore Acidification of Autophago-Lysosomes and Bacterial
760 Clearance in Cystic Fibrosis Macrophages. *Front Cell Infect Microbiol* **12**, 819554 (2022).
761 65. W. McAlpine *et al.*, Excessive endosomal TLR signaling causes inflammatory disease in mice
762 with defective SMCR8-WDR41-C9ORF72 complex function. *Proc Natl Acad Sci U S A* **115**,
763 E11523-e11531 (2018).
764 66. O. de Bouteiller *et al.*, Recognition of double-stranded RNA by human toll-like receptor 3 and
765 downstream receptor signaling requires multimerization and an acidic pH. *J Biol Chem* **280**,
766 38133-38145 (2005).
767 67. J. H. Zhang, Y. Qin, S. C. Sun, TMEM206 gene knockout improves balance performance in SCA1
768 transgenic mice. *IBRO Neurosci Rep* **19**, 996-999 (2025).

68. S. Kappel *et al.*, CBA (4-chloro-2-(2-chlorophenoxy)acetamido) benzoic acid) inhibits TMEM206 mediated currents and TMEM206 does not contribute to acid-induced cell death in colorectal cancer cells. *Front Pharmacol* **15**, 1369513 (2024).
69. K. Melek, B. Hauert, S. Kappel, TMEM206 Contributes to Cancer Hallmark Functions in Colorectal Cancer Cells and Is Regulated by p53 in a p21-Dependent Manner. *Cells* **13** (2024).
70. F. Peng, H. Li, J. Li, Z. Wang, Downregulation of the Proton-Activated Cl- Channel TMEM206 Inhibits Malignant Properties of Human Osteosarcoma Cells. *Oxid Med Cell Longev* **2021**, 3672112 (2021).
71. L. Song, D. Feng, J. Tan, H. Zhang, Effects of TMEM206 on the malignant behavior of HepG2 human hepatocellular carcinoma cells. *European Journal of Inflammation* **20**, 1721727X221122724 (2022).
72. L. Zhang, S. Y. Liu, X. Yang, Y. Q. Wang, Y. X. Cheng, TMEM206 is a potential prognostic marker of hepatocellular carcinoma. *Oncol Lett* **20**, 174 (2020).
73. Z. J. Yang, S. Y. Huang, Y. F. Zhou, S. C. Sun, Knockout of TMEM206 in mice associated with a loss of corneal transparency. *Int J Ophthalmol* **17**, 1967-1972 (2024).
74. K. H. Chen, T. Hagino, Z. Qiu, The Proton-Activated Chloride Channel: Molecular Identification, Structure, and Role in Organelle Physiology. *Annu Rev Physiol* 10.1146/annurev-physiol-022724-105357 (2025).
75. S. Gururaja Rao, N. J. Patel, H. Singh, Intracellular Chloride Channels: Novel Biomarkers in Diseases. *Front Physiol* **11**, 96 (2020).
76. S. Gururaja Rao, D. Ponnalagu, N. J. Patel, H. Singh, Three Decades of Chloride Intracellular Channel Proteins: From Organelle to Organ Physiology. *Curr Protoc Pharmacol* **80**, 11.21.11-11.21.17 (2018).
77. L. Mihaljević, Z. Ruan, J. Osei-Owusu, W. Lü, Z. Qiu, Inhibition of the proton-activated chloride channel PAC by PIP(2). *Elife* **12** (2023).
78. H. Y. Cheng *et al.*, The phagosome-mediated anti-bacterial immunity is governed by the proton-activated chloride channel in peritoneal macrophages. *bioRxiv* 10.1101/2025.02.27.640612, 2025.2002.2027.640612 (2025).
79. A. C. Ericsson, C. L. Franklin, The gut microbiome of laboratory mice: considerations and best practices for translational research. *Mamm Genome* **32**, 239-250 (2021).
80. V. M. Ripoll *et al.*, Nicotinamide nucleotide transhydrogenase (NNT) acts as a novel modulator of macrophage inflammatory responses. *Faseb j* **26**, 3550-3562 (2012).
81. J. Osei-Owusu *et al.*, Molecular mechanism underlying desensitization of the proton-activated chloride channel PAC. *Elife* **11** (2022).
82. B. Boilly, A. S. Vercoutter-Edouart, H. Hondermarck, V. Nurcombe, X. Le Bourhis, FGF signals for cell proliferation and migration through different pathways. *Cytokine Growth Factor Rev* **11**, 295-302 (2000).